



Online characterization of primary and secondary emissions of particulate matter and acidic molecules from a modern fleet of city buses

Liyuan Zhou^{1,2,★}, Qianyun Liu^{2,a,★}, Christian M. Salvador^{3,b}, Michael Le Breton^{3,c}, Mattias Hallquist³, Jian Zhen Yu⁴, Chak K. Chan^{1,2}, and Åsa M. Hallquist⁵

¹Division of Physical Science and Engineering, King Abdullah University of Science and Technology, Thuwal, Saudi Arabia

²School of Energy and Environment, City University of Hong Kong, Hong Kong SAR, China

³Department of Chemistry and Molecular Biology, University of Gothenburg, Gothenburg, Sweden

⁴Division of Environment and Sustainability, Hong Kong University of Science and Technology, Hong Kong SAR, China

⁵IVL Swedish Environmental Research Institute, Gothenburg, Sweden

^anow at: RELX Science Center, Shenzhen RELX Tech. Co., Ltd., Shenzhen, China

^bnow at: Environmental Sciences Division, Oak Ridge National Laboratory, Oak Ridge, TN 37830, USA

^cnow at: FEV Sverige AB, Gothenburg, Sweden

★These authors contributed equally to this work.

Correspondence: Chak K. Chan (chak.chan@kaust.edu.sa) and Åsa M. Hallquist (asa.hallquist@ivl.se)

Received: 19 February 2024 – Discussion started: 22 May 2024

Revised: 31 July 2024 – Accepted: 18 August 2024 – Published: 2 October 2024

Abstract. The potential impact of transitioning from conventional fossil fuel to a non-fossil-fuel vehicle fleet was investigated by measuring primary emissions via extractive sampling of bus plumes and assessing secondary mass formation using the Gothenburg Potential Aerosol Mass (Go:PAM) reactor from 76 in-use transit buses. Online chemical characterization of gaseous and particulate emissions from these buses was conducted using chemical ionization mass spectrometry (CIMS) with acetate as the reagent ion, coupled with the Filter Inlet for Gases and AEROSols (FIGAERO). Acetate reagent ion chemistry selectively ionizes acidic compounds, including organic and inorganic acids, as well as nitrated and sulfated organics. A significant reduction (48 %–98 %) in fresh particle emissions was observed in buses utilizing compressed natural gas (CNG), biodiesels like rapeseed methyl ester (RME) and hydrotreated vegetable oil (HVO), and hybrid-electric HVO (HVO_{HEV}) compared to diesel (DSL). However, secondary particle formation from photooxidation of emissions was substantial across all the fuel types. The median ratio of particle mass emission factors of aged to fresh emissions increased in the following order: DSL buses at 4.0, HVO buses at 6.7, HVO_{HEV} buses at 10.5, RME buses at 10.8, and CNG buses at 84. Of the compounds that can be identified by CIMS, fresh gaseous emissions from all Euro V/EEV (Enhanced Environmentally friendly Vehicle) buses, regardless of fuel type, were dominated by nitrogen-containing compounds such as nitrous acid (HONO), nitric acid (HNO₃), and isocyanic acid (HNCO), alongside small monoacids (C₁–C₃). Notably, the emission of nitrogen-containing compounds was lower in Euro VI buses equipped with more advanced emission control technologies. Secondary gaseous organic acids correlated strongly with gaseous HNO₃ signals ($R^2 = 0.85$ – 0.99) in Go:PAM, but their moderate to weak correlations with post-photooxidation secondary particle mass suggest that they are not reliable tracers of secondary organic aerosol formation from bus exhaust. Our study highlights that non-regulated compounds and secondary pollutant formation, not currently addressed in legislation, are crucial considerations in the evaluation of environmental impacts of future fuel and engine technology shifts.

1 Introduction

Air pollution remains a critical global issue, posing significant threats to both human health and the environment. Despite substantial progress in reducing emissions from major sources like industry, energy production, households, transportation, and agriculture, the worldwide achievement of air quality targets continues to be a daunting challenge. Notably, the road transportation sector, particularly in urban environments, significantly contributes to the emissions of nitrogen oxides (NO_x) and particulate matter (PM), impacting the health of individuals in densely populated regions. In tandem with these concerns, efforts to combat climate change have spurred an increase in the adoption of renewable energy sources within the transportation sector. Biodiesel has become the most prevalent renewable fuel, followed by bio-gas and ED95 ethanol (Guerreiro et al., 2014). Moreover, numerous cities are progressively integrating hybrid-electric and electric vehicles into their public transport fleets, aiming to reduce emissions.

Emissions from vehicles, especially buses, exhibit considerable variability. They are influenced by fuel type, engine design, operational conditions, emission after-treatment technologies, and maintenance (Pirjola et al., 2016; Zhao et al., 2018; Watne et al., 2018; Q. Liu et al., 2019; Zhou et al., 2020). While diesel (DSL) buses are common, there is an increasing trend towards the use of alternative fuels such as compressed natural gas (CNG), rapeseed methyl ester (RME), and hydrotreated vegetable oil (HVO). These alternative fuels offer several benefits, including reduced PM emissions (particularly of soot) and lower levels of carbon monoxide (CO) and total hydrocarbons (THCs) (Pflaum et al., 2010; Hassaneen et al., 2012; Q. Liu et al., 2019). However, the efficacy of RME and HVO in diminishing NO_x emissions can be inconsistent (Pirjola et al., 2016; Q. Liu et al., 2019), and CNG buses exhibit considerable variability in particle number (PN) emissions (Watne et al., 2018). In Sweden, approximately 23 % of the fuel mix of the transportation sector in 2020 comprised renewable fuels, with HVO accounting for over half of this proportion (Vourliotakis and Platsakis, 2022; Energimyndigheten, 2021). Emission control strategies, such as after-treatment systems including diesel particulate filters (DPFs) and selective catalytic reduction (SCR) systems, have been implemented to mitigate pollutant emissions from vehicles. These systems have shown significant efficacy in reducing PM and NO_x emissions, respectively, though their performance can vary under different operational conditions.

Accurately determining vehicle emission factors (EFs) is crucial for devising and implementing effective air quality policies (Fitzmaurice and Cohen, 2022). Methods such as chassis dynamometer tests, on-board measurements with a portable emission measurement system (PEMS), and on-road

vehicle chasing experiments have been employed to assess emissions from various types of vehicles (Kwak et al., 2014; Ježek et al., 2015; Pirjola et al., 2016). Chassis dynamometer tests offer high repeatability over standard driving cycles but may not reflect real-world driving conditions or fleet maintenance levels. There are also challenges in accurately replicating real-world dilution effects (Vogt et al., 2003; Kuittinen et al., 2021). On-board measurements with a PEMS provide data under a wide range of operating conditions, yet like dynamometers they may not realistically mimic ambient dilution processes (Giechaskiel et al., 2015; Wang et al., 2020). On-road vehicle chasing experiments involve following individual vehicles with a mobile laboratory to capture the exhaust plumes, providing insights into realistic dilution processes from the tailpipe to ambient air, though these experiments often require a test track to ensure traffic safety (Wang et al., 2020; Tong et al., 2022). All three methods are limited by small sample sizes, which constrain understanding of the real emission characteristics of vehicle fleets. Alternatively, roadside or near-road measurements provide the ability to monitor emissions from a large number of vehicles under actual driving conditions within a short time frame (Hallquist et al., 2013; Watne et al., 2018; Q. Liu et al., 2019), which is particularly important for assessing exposure risks to pedestrians and bus passengers. However, this method is limited by its inability to monitor specific engines or operational conditions, such as varying engine speeds and loads. Integrating results from diverse methodologies would ideally yield a comprehensive understanding of emissions from vehicle transport systems.

In a prior study, we conducted roadside point measurements and reported EFs for general air pollutants such as PM, NO_x , CO, and THCs from individual buses during stop-and-go operations at a bus stop in Gothenburg, Sweden (Q. Liu et al., 2019). Our findings showed that hybrid buses, when using their combustion engines to accelerate from a standstill at bus stops, tended to emit higher PNs than traditional DSL buses, likely due to their relatively smaller engines. Expanding on our prior findings, it is important to acknowledge that primary emissions are not the only way in which engine emissions impact air quality. Emissions from engine exhaust can contribute to secondary particles through oxidation of gas-phase species, primarily via functionalization reactions, yielding lower-volatility products (Hallquist et al., 2009; Kroll et al., 2009). Laboratory studies have demonstrated that secondary organic aerosols (SOA) produced from diluted vehicle exhaust frequently exceed the levels of primary organic aerosols (POA) in less than 1 d of atmospheric equivalent aging (Chirico et al., 2010; Nordin et al., 2013; Platt et al., 2013; Gordon et al., 2014b; Liu et al., 2015). Oxidation flow reactors (OFRs) enable the simulation of several days of atmospheric aging in a few minutes, with minimized wall effects compared to traditional smog chamber experi-

ments (Palm et al., 2016; Bruns et al., 2015). OFRs have been extensively employed to assess the SOA formation potential of ambient air and emissions from diverse sources, including motor exhausts (Tkacik et al., 2014; Bruns et al., 2015; Simonen et al., 2017; Watne et al., 2018; T. Liu et al., 2019; Kuittinen et al., 2021; Zhou et al., 2021; Liao et al., 2021; Yao et al., 2022). In real-world traffic scenarios, the rapid response capabilities and convenient deployment of OFRs, coupled with roadside point measurements, provide a robust method for evaluating emissions from a significant number of vehicles. This approach effectively captures the considerable variability among the individual vehicles within a fleet, offering a comprehensive view of emissions under actual driving conditions (Watne et al., 2018; Zhou et al., 2021), although this may not encompass as extensive a range of engine operations as setups that integrate OFRs with chassis dynamometer tests (Kuittinen et al., 2021).

Primary emissions can also be oxidized to higher-volatility products through fragmentation reactions, potentially producing carboxylic acids (Friedman et al., 2017). Engine exhaust is a recognized primary source of organic and inorganic acids in urban environments (Kawamura et al., 1985; Kawamura and Kaplan, 1987; Kirchstetter et al., 1996; Wentzell et al., 2013; Friedman et al., 2017). Monocarboxylic acids are produced by both diesel and spark-ignited engines (Kawamura et al., 1985; Zervas et al., 2001a; Zervas et al., 2001b; Crisp et al., 2014). Recent studies have identified gaseous dicarboxylic acids in diesel exhaust (Arnold et al., 2012), compounds likely linked to the nucleation and growth of particles (Zhang et al., 2004; Pirjola et al., 2015). Additionally, inorganic acids such as the nitric (HNO_3) and nitrous (HONO) acids, along with isocyanic acid (HNCO) – implicated in serious health issues like atherosclerosis, cataracts, and rheumatoid arthritis through carbamylation reactions (Fullerton et al., 2008; Roberts et al., 2011) – have been identified in both diesel and gasoline exhausts (Wang et al., 2007; Roberts et al., 2011; Wentzell et al., 2013; Brady et al., 2014; Link et al., 2016; Li et al., 2021). However, the secondary production of organic acids from engine exhaust remains poorly characterized, and it may significantly contribute to the overall organic acid budget and help explain discrepancies between models and measurements (Paulot et al., 2011; Millet et al., 2015; Yuan et al., 2015). Furthermore, the impacts of evolving fuel and engine technologies on emissions have not been comprehensively assessed. Recent advances in analytical techniques now enable simultaneous, high-resolution online measurements of both gas- and particle-phase acidic species. This is facilitated by high-resolution time-of-flight chemical ionization mass spectrometry (HR-ToF-CIMS) using acetate as the reagent ion, coupled with the Filter Inlet for Gases and AEROSols (FIGAERO) (Le Breton et al., 2019; Friedman et al., 2017; Lopez-Hilfiker et al., 2014).

In this study, we employed the OFR Gothenburg Potential Aerosol Mass Reactor (Go:PAM) along with roadside point

measurements to capture emissions from a diverse array of fuel types and engine technologies in in-use transit buses. We present findings on the photochemical aging of emissions from a modern fleet operating on DSL and the latest generation of alternative fuels, including CNG, RME, and HVO. Our study aims to compare the secondary production of PM from individual buses in real traffic scenarios to their primary PM emissions, examining the impact of fuel type, engine technology, and photochemical age. Furthermore, both fresh and aged emissions of the gas and particle phases are characterized using HR-ToF-CIMS, providing a comprehensive understanding of the emission profile and its environmental implications.

2 Methods

2.1 Emission measurements

Roadside measurements were conducted at a designated urban bus stop, featuring a bus-only lane, in Gothenburg, Sweden (Supplement Fig. S1). The sampling occurred from 2 to 12 March 2016, with the average temperature during this period was recorded at approximately 3.9 °C. Extractive sampling of individual bus plumes in real traffic was used to characterize emissions, adhering to the method outlined by Hallquist et al. (2013). Air was continuously drawn through a cord-reinforced flexible conductive hose to the instruments housed within a nearby container. Additional details of the experimental conditions are available in our prior publication Q. Liu et al. (2019). The primary focus of this study was to utilize the OFR Go:PAM and the HR-ToF-CIMS to explore the potential for secondary pollutant formation and to conduct a detailed chemical characterization of both gas- and particle-phase compounds. An experimental schematic of the roadside sampling is shown in Fig. S2 in the Supplement. Briefly, the emissions from passing bus plumes were characterized as they accelerated from standstill at the bus stop. A camera was positioned on the roadside to capture bus plate numbers, facilitating bus identification and enabling the collection of specific information on each bus, including fuel type, engine technology, and exhaust after-treatment systems. The effective identification of emissions from individual buses was achieved by employing CO_2 as a tracer, as delineated by Hak et al. (2009). The concentration of CO_2 was measured with a nondispersive infrared gas analyzer (LI-840 A, time resolution 1 Hz). NO and NO_x were measured with two separate chemiluminescent analyzers (Thermo Scientific™ Model 42i $\text{NO}-\text{NO}_2-\text{NO}_x$ Analyzer). In addition, specific gaseous compounds like CO , NO , and THCs were measured using a remote sensing device (AccuScan RSD 3000, Environmental System Products Inc.). Particle emissions were characterized using the high-time-resolution Engine Exhaust Particle Sizer Spectrometer (EEPS, Model 3090, TSI Inc., time resolution 10 Hz) across a size range of 5.6–560 nm. Due to the lack of detailed knowl-

edge about the chemical composition of the emitted particles, particle mass calculations were based on the assumption of spherical particles of unit density.

The HR-ToF-CIMS coupled with FIGAERO was used to derive chemical information of both gas- and particle-phase species. A detailed description of the configuration of the instrument can be found elsewhere (Aljawhary et al., 2013; Lopez-Hilfiker et al., 2014; Le Breton et al., 2018; Le Breton et al., 2019). Acetate, employed as the reagent ion, was generated using an acetic anhydride permeation source through a ^{210}Po ion source (^{210}Po inline ionizer, NRD inc, Static Solutions Limited). In the ion–molecule reaction (IMR) chamber, the gaseous sampling flow interacted with the reagent ions, leading to the ionization of the target molecules. The dual inlets of FIGAERO enable simultaneous gas-phase sampling directly into the IMR chamber and particle sample collection on a PTFE filter for the duration of the plume via a separate inlet. The duration of the target plume for particle collection was indicated by a PN concentration measured by the EEPS. Once the PN concentration became indistinguishable at background levels, the filter was automatically positioned to allow the collected particles to be evaporated into the IMR chamber. The nitrogen flow over the filter was incrementally heated from room temperature to 200 °C within 5 min and then maintained at this maximum temperature for 8 min, ensuring complete desorption of mass from the filter, followed by analysis using HR-ToF-CIMS. Perfluoropentanoic acid (PFPA), a reliable high-mass calibrant, was injected into the CIMS inlet during the sampling period (Le Breton et al., 2019). Mass spectra were calibrated using known masses (m/z) accurate to within 4 ppm: O_2^- , CNO^- , $\text{C}_3\text{H}_5\text{O}_3^-$, $\text{C}_2\text{F}_3\text{O}_3^-$, $\text{C}_5\text{F}_9\text{O}_2^-$, and $\text{C}_{10}\text{F}_{18}\text{O}_4^-$ covered a range of 32–526 m/z (more details can be found in the Supplement). The data were acquired at a 1 s time resolution. To estimate the absolute EFs, a conversion of CIMS signal to concentration using a sensitivity factor is necessary. Based on the method of Lopez-Hilfiker et al. (2015), the maximum sensitivity was determined to be 20 Hz ppt $^{-1}$, which falls within previously reported ranges (Mohr et al., 2017). Using this maximum sensitivity provides a lower-limit estimate of EFs for all oxygenated volatile organic compounds (Zhou et al., 2021). The assumption of sensitivity did not affect the comparative analysis of EFs with respect to different fuel types.

The EFs of constituents per kilogram of fuel burned were calculated by relating the concentration change of a specific compound in the diluted exhaust plume to the change in the CO_2 concentration. CO_2 served as a tracer for exhaust gas dilution relative to the background concentration (Janhäll and Hallquist, 2005; Hak et al., 2009; Hallquist et al., 2013; Watne et al., 2018). Assumptions were made for complete combustion, and carbon contents of 86.1%, 77.3%, 70.5%, and 69.2 % for DSL, RME, HVO, and CNG, respectively, were assumed (Edwards et al., 2004). Further methodological details are elaborated on in Q. Liu et al. (2019). A more

comprehensive description of the EF calculations is provided in the Supplement.

2.2 Oxidation flow reactor setup

The OFR Go:PAM was utilized for photochemical aging of emissions from individual buses to investigate the potential for secondary pollutant formation. The comprehensive description and operational protocols of Go:PAM have been detailed previously (Watne et al., 2018; Zhou et al., 2021). Briefly, Go:PAM is a 6.1 L continuous-flow quartz glass flow reactor with input flows such that the median residence time is approximately 37 s. The reactor is equipped with two Philips TUV 30 W fluorescent lamps ($\lambda = 254$ nm) and enclosed by reflective and polished aluminum mirrors to ensure a homogeneous photon field. The UV lamps generate OH radicals through the photolysis of O_3 in the presence of water vapor. The relative humidity (RH) within the reactor was around 60–80 %. The O_3 concentration inside Go:PAM was measured using an ozone monitor (2B Technologies, Model 205 dual-beam ozone monitor) at around 880 ppb prior to the introduction of vehicle exhaust. Particle wall losses in Go:PAM were corrected using size-dependent transmission efficiency (Watne et al., 2018). The OH exposure (OH_{exp}) inside Go:PAM was calibrated offline using sulfur dioxide (SO_2) and following methodologies established in previous studies (Lambe et al., 2011; Kang et al., 2007), with additional details provided in the Supplement. During on-road measurements, OH_{exp} may be significantly influenced by OH reactivity (i.e., CO and HC) and titration of O_3 by NO in the plumes, which varied between vehicles. Thus, the OH reactivity was estimated for each bus passage using the maximum NO_x , CO, and HC concentrations in Go:PAM along with the corresponding water and ozone levels (Watne et al., 2018; Zhou et al., 2021). Employing the maximum concentrations of these OH- or O_3 -consuming species represents a minimum estimate of OH_{exp} in our calculations. The flow design incorporated into Go:PAM enables investigation of transient phenomena, such as passing plumes. It also works at relatively low ozone concentrations (less than 1 ppm), limiting the reactions of other potential oxidants such as O_3 , NO_3 , or O^1D (Zhou et al., 2021).

3 Results and discussion

3.1 Fresh and aged PM emissions from buses

The aged PM emissions ($\text{EF}_{\text{PM:aged}}$) of 133 plumes from a diverse set of buses, including 16 diesel (DSL), 11 compressed natural gas (CNG), 20 rapeseed methyl ester (RME), 20 hydrotreated vegetable oil (HVO), and 9 hybrid-electric HVO (HVO_{HEV}) buses, were investigated using Go:PAM. The corresponding average fresh PM emissions ($\text{EF}_{\text{PM:Fresh}}$) for these 76 buses were measured during several sequential days (Fig. S2). These buses were a subset of the 234 buses

described in our previous study (Q. Liu et al., 2019) and represent data corresponding to available Go:PAM measurements. A comprehensive discussion on the full dataset for fresh conditions is available in Q. Liu et al. (2019). Figure 1 shows the average $EF_{PM:Fresh}$ and $EF_{PM:aged}$ with respect to fuel type. Among the buses, Euro V DSL models had the highest median $EF_{PM:Fresh}$, $MdEF_{PM:Fresh}$ (represented by the horizontal yellow lines), of $208 \text{ mg (kg fuel)}^{-1}$, followed by HVO_{HEV}, RME, and HVO buses with $MdEF_{PM:Fresh}$ values of 109, 74, and $62 \text{ mg (kg fuel)}^{-1}$, respectively. CNG buses and HVO_{HEV} buses equipped with a DPF under Euro VI standards exhibited the lowest $MdEF_{PM:Fresh}$, with over half of these buses exhibiting $EF_{PM:Fresh}$ below the detection limit ($< 4.3 \text{ mg (kg fuel)}^{-1}$). Except for HVO_{HEV} buses with a DPF, which was limited to a small tested number, all other bus types in this subset had a $MdEF_{PM:Fresh}$ comparable to those of the full dataset in Q. Liu et al. (2019), within $\pm 30\%$ and following the same rank order. The average EFs of fresh and aged particle emissions and the general gaseous pollutants for the individual buses are given in Table 1.

After photooxidation in Go:PAM, particle mass increased markedly, with half of the individual buses showing an average $EF_{PM:aged}$ of more than 8 times their average $EF_{PM:Fresh}$. For all Euro V/EEV (Enhanced Environmentally friendly Vehicle) buses, the median $EF_{PM:aged}$, i.e., $MdEF_{PM:aged}$ (represented by the horizontal blue lines), was highest for DSL buses with $749 \text{ mg (kg fuel)}^{-1}$, followed by a descending order of RME (655) > CNG(645) > HVO(543) > HVO_{HEV} (509). Despite the low $EF_{PM:Fresh}$, CNG buses produced substantial secondary particle mass. The DPF, proven effective in earlier studies (Martinet et al., 2017; Preble et al., 2015; May et al., 2014), efficiently reduced primary particle emissions from the DSL Euro III and HVO_{HEV} Euro VI buses. However, these bus types, even with DPFs, exhibited a higher $EF_{PM:aged}$ than those using the same fuels but without DPFs (Euro V), although the number of tested buses with DPFs was limited. The variance in the median $EF_{PM:aged}$ among the different fuel types was less pronounced compared to $EF_{PM:Fresh}$, suggesting the presence of significant non-fuel-dependent precursor sources, such as lubrication oils and/or fuel additives (Watne et al., 2018; Le Breton et al., 2019).

Figure 2 shows the bus average $EF_{PM:Fresh}$ vs. the corresponding $EF_{PM:aged}$ for individual bus passages, where the average $EF_{PM:aged}$ for each bus is indicated by a solid horizontal line. This analysis focuses on Euro V/EEV buses to ensure a sufficient number of buses in the comparison, while buses from the other Euro classes were not included due to their limited numbers. The median ratio of $EF_{PM:aged}$ to $EF_{PM:Fresh}$ was highest for CNG buses (84), followed by RME (10.8), HVO_{HEV} (10.5), HVO (6.7), and DSL(4.0) buses. Buses equipped with DPFs, such as DSL Euro III and HVO_{HEV} Euro VI (not included in Fig. 2), exhibited a median ratio exceeding 50. $EF_{PM:aged}$ exhibited notable variation between passages of the same bus, likely attributable to emission variability between passages and different dilution

levels for plumes prior to sampling into Go:PAM. This is illustrated in Fig. 2b, where $EF_{PM:Fresh}$ and $EF_{PM:aged}$ are presented as a function of the dilution level, which is indicated by the integrated CO_2 area. Generally, a higher integrated CO_2 area suggests a more concentrated plume, leading to increased external OH and O_3 reactivity, which in turn reduces the concentrations of OH radicals available in Go:PAM for precursor oxidation (Emanuelsson et al., 2013; Watne et al., 2018). Some buses displayed primary emissions too dilute for detection (markers located to the left in Fig. 2b), but they still exhibited non-negligible $EF_{PM:aged}$ after oxidation. To further examine the effects of simulated atmospheric oxidation in Go:PAM, an estimated minimum OH_{exp} was calculated for each plume by incorporating the OH reactivities of CO and HC and the titration of O_3 with NO, following the methodologies of Watne et al. (2018) and Zhou et al. (2021). For all plumes, OH_{exp} varied between 1.1×10^9 and $4.6 \times 10^{11} \text{ molecules cm}^{-3} \text{ s}$. The $EF_{PM:aged}$ for some buses, for example the DSL and HVO located to the right in Fig. 2c, increased with increasing OH_{exp} . However, due to potential large differences in the chemical composition of emissions across different passages of the same bus, where some species are more prone to forming secondary particle mass even at lower OH_{exp} , the OH_{exp} -dependent $EF_{PM:aged}$ for the other buses was less pronounced.

The secondary particle mass formed (ΔPM) was calculated as the difference between $EF_{PM:aged}$ for a plume and the average $EF_{PM:Fresh}$ for the corresponding individual bus. Figure 3 illustrates ΔPM as a function of OH_{exp} for the bus fleet in this study, which includes 40 % DSL, 12.2 % CNG, 20 % RME, 20.8 % HVO, and 7 % HVO_{HEV}. The results were grouped based on OH_{exp} , spanning a range from 1.1×10^9 to $4.6 \times 10^{11} \text{ molecules cm}^{-3} \text{ s}$. The results in this study are compared with those reported by a tunnel study (Tkacik et al., 2014), an urban roadside study of a mixed fleet in Hong Kong (T. Liu et al., 2019), a depot study on rather modern types of city buses (Watne et al., 2018), and roadside measurements of a heavy-duty truck fleet in Gothenburg (Zhou et al., 2021). Laboratory OFR and chamber studies of middle-duty and heavy-duty diesel vehicles (Deng et al., 2017), diesel passenger cars (Chirico et al., 2010), a diesel engine (Jathar et al., 2017a), and gasoline vehicles (Gordon et al., 2014a; Platt et al., 2013) were also included for comparison. Note that ΔPM in this study, alongside those of Watne et al. (2018), Zhou et al. (2021), and T. Liu et al. (2019), includes both secondary organic and inorganic aerosol, while ΔPM in research by Deng et al. (2017), Chirico et al. (2010), Jathar et al. (2017a), Gordon et al. (2014a), Platt et al. (2013), and Tkacik et al. (2014) pertains only to secondary organic aerosol mass.

The ΔPM from vehicle emissions is influenced by factors such as vehicle and fuel types, driving modes, and OH_{exp} during experiments (Gentner et al., 2017). Considering the variability of OH reactivity among vehicles and the consequently wide range of OH_{exp} , this study,

Table 1. Average particle and gaseous EFs of individual buses for fresh emissions and the average EF_{PM} for aged emissions^a.

| Bus ID | Fuel ^c | Euro standard | Exhaust after-treatment system ^d | EF _{PM:Fresh} (mg (kg fuel) ⁻¹) | EF _{PN:Fresh} (10 ¹⁴ particles (kg fuel) ⁻¹) | EF _{CO} (g (kg fuel) ⁻¹) | EF _{THC} (g (kg fuel) ⁻¹) | EF _{NO_x} (g (kg fuel) ⁻¹) | EF _{PM:Aged} (mg (kg fuel) ⁻¹) |
|--------|-------------------|---------------|---|--|--|---|--|---|---|
| 1 | DSL | III | SCR, DPF | 4.3 | 0.41 | 3.9 ± 11 | 1.5 ± 2.9 | 10 ± 3.2 | 810 ± 510 |
| 2 | DSL | III | SCR, DPF | 120 ± 190 | 34 ± 61 | 2.7 ± 7 | 1.7 ± 3.7 | 11 ± 5 | 1300 |
| 3 | DSL | V | SCR | 130 ± 45 | 3.3 ± 1.3 | 17 ± 18 | 0.35 ± 1.3 | 3.9 ± 3.7 | 160 ± 13 |
| 4 | DSL | V | SCR | 130 | 3.6 | 20 ± 22 | 1.5 ± 3.6 | 4.7 ± 7.2 | 230 ± 100 |
| 5 | DSL | V | SCR | 320 | 5.9 | 20 ± 28 | 2 ± 3.5 | 9.7 ± 7 | 430 ± 23 |
| 6 | DSL | V | SCR | 78 | 1.6 | 20 ± 21 | 2.7 ± 5.6 | 13 ± 12 | 480 |
| 7 | DSL | V | SCR | 670 ± 350 | 10 ± 6.8 | 42 ± 44 | 2.3 ± 3.7 | 6.8 ± 5 | 570 ± 92 |
| 8 | DSL | V | SCR | 190 ± 110 | 6.5 ± 3 | 14 ± 21 | 0.75 ± 1.7 | 12 ± 5.1 | 620 ± 530 |
| 9 | DSL | V | SCR | 140 ± 130 | 4.3 ± 2.6 | 9.8 ± 14 | 1 ± 1.5 | 15 ± 13 | 680 ± 260 |
| 10 | DSL | V | SCR | 120 ± 4.7 | 3.2 ± 0.66 | 16 ± 18 | 2.5 ± 4.7 | 12 ± 6.9 | 820 ± 160 |
| 11 | DSL | V | SCR | 250 ± 140 | 4.7 ± 2.7 | 16 ± 23 | 0.8 ± 1.4 | 12 ± 8.9 | 900 ± 1000 |
| 12 | DSL | V | SCR | 230 ± 120 | 5.1 ± 1.5 | 16 ± 26 | 2.6 ± 4.6 | 12 ± 9.9 | 1000 ± 620 |
| 13 | DSL | V | SCR | 160 ± 41 | 3.5 ± 0.97 | 27 ± 27 | 1.4 ± 2.7 | 17 ± 9.8 | 1000 ± 540 |
| 14 | DSL | V | SCR | 220 ± 110 | 5.2 ± 1.3 | 12 ± 17 | 2.6 ± 4.1 | 11 ± 7.4 | 1100 ± 1100 |
| 15 | DSL | V | SCR | 360 ± 130 | 6.8 ± 4.2 | 21 ± 25 | 1.2 ± 3.3 | 5.7 ± 4.4 | 1200 |
| 16 | DSL | V | SCR | 240 ± 220 | 22 ± 11 | 5.5 ± 7.5 | 0.74 ± 1.6 | 6.8 ± 5.6 | 4200 |
| 17 | CNG | EEV | – | 4.3 ± 0 | 0.41 ± 0 | NA | NA | 4.8 ± 1.7 | 200 |
| 18 | CNG | EEV | – | NA | NA | NA | NA | 11 ± 4.9 | 360 |
| 19 | CNG | EEV | – | 4.3 ± 0 | 0.41 ± 0 | NA | NA | 4 ± 3.8 | 520 |
| 20 | CNG | EEV | – | NA | NA | NA | NA | 15 ± 17 | 560 |
| 21 | CNG | EEV | – | 28 | 1.3 | NA | NA | 2.2 ± 0.93 | 590 |
| 22 | CNG | EEV | – | 4.3 | 0.41 | NA | NA | 1.8 ± 1 | 650 ± 140 |
| 23 | CNG | EEV | – | NA | NA | NA | NA | 3.2 ± 0.53 | 700 |
| 24 | CNG | EEV | – | 4.3 | 0.41 | NA | NA | 6.9 ± 1.4 | 950 ± 900 |
| 25 | CNG | EEV | – | 38 | 11 | NA | NA | 7.3 ± 5.3 | 1100 ± 750 |
| 26 | CNG | EEV | – | 110 | 200 | NA | NA | 8.2 ± 4.2 | 1200 ± 480 |
| 27 | CNG | EEV | – | 4.3 ± 0 | 0.41 ± 0 | NA | NA | 6 ± 1.8 | 1600 |
| 28 | RME | IV | SCR | NA | NA | 10 ± 8.7 | 3.1 ± 3 | 46 ± 20 | 850 |
| 29 | RME | IV | SCR | 110 | 4.1 | 4.2 ± 8.4 | 0.19 ± 0.38 | 7.2 ± 6.8 | 3000 |
| 30 | RME | V | SCR | 44 | 2.2 | 12 ± 14 | 2.2 ± 3.6 | 32 ± 32 | 140 |
| 31 | RME | V | SCR | 4.3 | 0.41 | 7.4 ± 7.1 | 0.075 ± 0.17 | 13 ± 5.1 | 170 |
| 32 | RME | V | SCR | 39 | 6.2 | 5.2 ± 4.8 | 0.87 ± 1.1 | 18 ± 5.4 | 210 |
| 33 | RME | V | SCR | NA | NA | 0.24 ± 0.54 | 0.24 ± 0.39 | 10 ± 3.3 | 320 |
| 34 | RME | V | SCR | 66 ± 11 | 2.4 ± 1 | 7 ± 7.2 | 1.8 ± 2.7 | 23 ± 13 | 370 ± 290 |
| 35 | RME | V | SCR | 8.6 | 0.96 | 4.9 ± 3.6 | 0.59 ± 0.73 | 20 ± 5.1 | 420 ± 75 |
| 36 | RME | V | SCR | 4.3 | 0.41 | 22 ± 23 | 1.8 ± 2 | 25 ± 16 | 520 |
| 37 | RME | V | SCR | 170 ± 7.7 | 6.4 ± 1 | 34 ± 35 | 0.016 ± 0.043 | 19 ± 10 | 550 |
| 38 | RME | V | SCR | 130 ± 24 | 11 ± 14 | 17 ± 20 | 2 ± 4 | 16 ± 15 | 590 |
| 39 | RME | V | SCR | NA | NA | 1.2 | 0.64 | 21 | 720 |
| 40 | RME | V | SCR | 120 | 5.3 | 12 ± 9.4 | 1.8 ± 2.6 | 18 ± 8.2 | 730 |
| 41 | RME | V | SCR | 80 ± 95 | 4.2 ± 2.9 | 8.8 ± 17 | 0.72 ± 0.87 | 25 ± 5.7 | 860 |
| 42 | RME | V | SCR | 470 | 5.8 | 4.5 ± 5.1 | 0.23 ± 0.38 | 18 ± 7.8 | 970 ± 210 |
| 43 | RME | V | SCR | 89 ± 2.3 | 2.6 ± 0.16 | 5.4 ± 9.4 | 0.68 ± 1.9 | 28 ± 17 | 1000 ± 210 |
| 44 | RME | V | SCR | 92 | 1.6 | 14 ± 19 | 1.8 ± 3 | 23 ± 17 | 1000 ± 420 |
| 45 | RME | V | SCR | NA | NA | 37 ± 26 | 5.8 ± 3.6 | 14 ± 6.3 | 1400 |
| 46 | RME | V | SCR | 4.3 ± 0 | 0.41 ± 0 | 9.6 ± 14 | 0.89 ± 1.4 | 28 ± 8.4 | 1500 ± 1800 |
| 47 | RME | V | SCR | 74 ± 75 | 12 ± 6 | 6.1 ± 6.3 | 1.1 ± 1.4 | 18 ± 5.2 | 1500 |
| 48 | HVO | V | SCR | 41 | 1.5 | 8.4 ± 2 | 0.14 ± 0.31 | 10 ± 0.4 | 31 |
| 49 | HVO | V | SCR | NA | NA | 5.8 ± 8 | 0.7 ± 0.62 | 13 ± 10 | 200 |
| 50 | HVO | V | SCR | 220 | 6.6 | 8.3 ± 9.1 | 0.91 ± 0.97 | 13 ± 8.6 | 220 |
| 51 | HVO | V | SCR | 79 ± 31 | 2.6 ± 0.74 | 7.8 ± 5.8 | 0.41 ± 0.59 | 12 ± 8.2 | 230 |
| 52 | HVO | V | SCR | 37 ± 13 | 1.9 ± 0.65 | 4.8 ± 5.5 | 0.64 ± 0.82 | 20 ± 3 | 240 ± 51 |
| 53 | HVO | V | SCR | 40 | 2.5 | 2.1 ± 3.4 | 0.0083 ± 0.019 | 16 ± 4.3 | 260 ± 160 |
| 54 | HVO | V | SCR | NA | NA | 2.1 ± 3 | 0.55 ± 0.77 | 22 | 270 |
| 55 | HVO | V | SCR | 46 ± 6.6 | 2.6 ± 0.52 | 6.2 ± 4.1 | 0.79 ± 0.55 | 12 ± 8.2 | 390 |
| 56 | HVO | V | SCR | NA | NA | 11 ± 10 | 0.74 ± 0.84 | 5.7 | 530 |
| 57 | HVO | V | SCR | NA | NA | 14 ± 17 | 0.79 ± 1.2 | 11 ± 2.6 | 540 |
| 58 | HVO | V | SCR | 62 | 4.1 | 6.8 ± 6.7 | 0.22 ± 0.31 | 11 ± 6.3 | 560 ± 660 |
| 59 | HVO | V | SCR | 76 | 5.3 | 2.3 ± 2 | 0.24 ± 0.47 | 19 ± 3.4 | 630 ± 700 |
| 60 | HVO | V | SCR | 35 ± 11 | 1.5 ± 0.19 | 3.3 ± 5 | 0.45 ± 0.86 | 9.2 ± 9 | 640 |

Table 1. Continued.

| Bus ID | Fuel ^c | Euro standard | Exhaust after-treatment system ^d | EF _{PM:Fresh} (mg (kg fuel) ⁻¹) | EF _{PN:Fresh} (10 ¹⁴ particles (kg fuel) ⁻¹) | EF _{CO} (g (kg fuel) ⁻¹) | EF _{THC} (g (kg fuel) ⁻¹) | EF _{NO_x} (g (kg fuel) ⁻¹) | EF _{PM:Aged} (mg (kg fuel) ⁻¹) |
|--------|--------------------|---------------|---|--|--|---|--|---|---|
| 61 | HVO | V | SCR | 280 | 14 | 9.9 ± 16 | 0.55 ± 0.73 | 11 ± 3.6 | 670 ± 160 |
| 62 | HVO | V | SCR | 190 ± 120 | 68 ± 86 | 1.1 ± 1.9 | 0.3 ± 0.49 | 9.3 ± 4.9 | 700 ± 570 |
| 63 | HVO | V | SCR | 54 ± 30 | 4.6 ± 2.2 | 3.5 ± 4.6 | 0.49 ± 0.48 | 14 ± 3.5 | 720 ± 310 |
| 64 | HVO | V | SCR | 4.3 | 0.41 | 2.2 ± 3.8 | 0.33 ± 0.73 | 12 ± 4.8 | 760 |
| 65 | HVO | V | SCR | 450 ± 220 | 18 ± 18 | 1.4 ± 1.6 | 0.28 ± 0.37 | 12 ± 2.6 | 1300 ± 720 |
| 66 | HVO | V | SCR | 81 | 11 | 0.88 ± 0.93 | 0.28 ± 0.25 | 13 ± 6.5 | 4100 |
| 67 | HVO | V | EGR, DPF | NA | NA | 4.6 ± 5.9 | 0.64 ± 1.2 | 11 ± 8.1 | 550 ± 150 |
| 68 | HVO _{HEV} | V | SCR | 130 | 52 | 12 ± 19 | 0.97 ± 1.4 | 20 ± 15 | 490 |
| 69 | HVO _{HEV} | V | SCR | NA | NA | 4.1 ± 8.4 | 0.5 ± 1.3 | 18 ± 3.3 | 500 ± 110 |
| 70 | HVO _{HEV} | V | SCR | 97 ± 100 | 25 ± 18 | 3.8 ± 6.8 | 1.1 ± 1.8 | 17 ± 5.7 | 500 ± 390 |
| 71 | HVO _{HEV} | V | SCR | NA | NA | 7.6 ± 9.9 | 2.9 ± 2.4 | 12 ± 2.1 | 520 |
| 72 | HVO _{HEV} | V | SCR | 4.3 ± 0 | 0.41 ± 0 | 3.7 ± 5.8 | 1 ± 2.4 | 20 ± 10 | 1100 |
| 73 | HVO _{HEV} | V | SCR | 120 ± 72 | 8.9 ± 2.9 | 1.2 ± 1.7 | 0.18 ± 0.26 | 17 ± 7 | 1900 |
| 74 | HVO _{HEV} | VI | SCR, EGR, DPF | 4.3 ± 0 | 0.41 ± 0 | 4.7 ± 11 | 2.2 ± 4.7 | 7.2 ± 8.5 | 240 |
| 75 | HVO _{HEV} | VI | SCR, EGR, DPF | 33 | 29 | 1.2 ± 2.4 | 0.22 ± 0.49 | 6.7 ± 3.3 | 550 |
| 76 | HVO _{HEV} | VI | SCR, EGR, DPF | 4.3 | 0.41 | 10 ± 9.2 | 1.5 ± 2.3 | 8.8 ± 8.7 | 4100 |

^a The given errors represent the standard deviation (1σ). ^b "NA" is the abbreviation for "not available". ^c DSL, CNG, RME, HVO, and HVO_{HEV} are the abbreviations for diesel, compressed natural gas, rapeseed methyl ester, hydrotreated vegetable oil, and hybrid-electric hydrotreated vegetable oil. ^d SCR, DPF, and EGR are the abbreviations for selective catalytic reduction, diesel particulate filter, and exhaust gas recirculation systems.

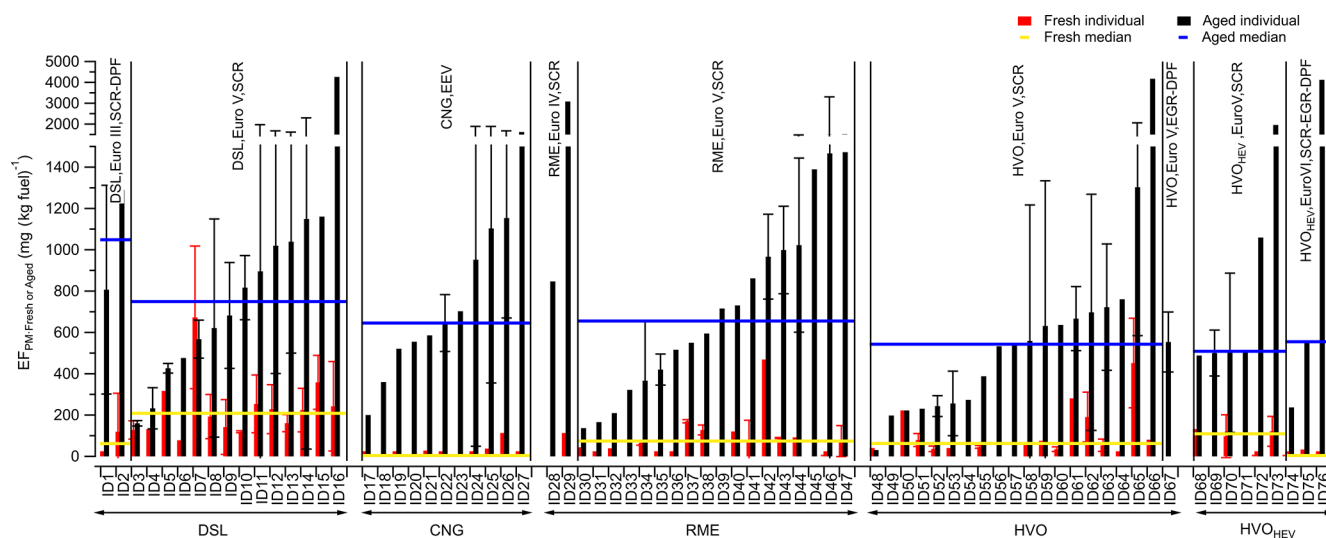


Figure 1. EF_{PM:Fresh} (red bar) and EF_{PM:aged} (black bar) with respect to fuel class: DSL (diesel, ID₁–ID₁₆), CNG (compressed natural gas, ID₁₇–ID₂₇), RME (rapeseed methyl ester, ID₂₈–ID₄₇), HVO (hydrotreated vegetable oil, ID₄₈–ID₆₇), and HVO_{HEV} (hybrid-electric HVO, ID₆₈–ID₇₆) buses. Median values for EF_{PM:Fresh} (M_d EF_{PM:Fresh}) and EF_{PM:aged} (M_d EF_{PM:aged}) are indicated by the horizontal yellow and blue lines, respectively. The information on the engine technology and exhaust after-treatment systems is also shown. The given errors represent the standard deviation (1σ).

along with Watne et al. (2018), categorizes Δ PM trends into OH_{exp} bins. The median Δ PM was approximately 400 mg (kg fuel)⁻¹ at OH_{exp} < 4.3 × 10¹⁰ molecules cm⁻³ s (corresponding to 1 OH day, assuming an OH concentration of 1 × 10⁶ molecules cm⁻³ for 12 h d⁻¹) and was 364–495 mg (kg fuel)⁻¹ at 1–5 OH days, reaching a maximum of around 920 mg (kg fuel)⁻¹ at approximately 5–6 OH days for the bus fleet in this study. This peak value of Δ PM was lower than the approximately 3000 mg (kg fuel)⁻¹ at ~5–6 OH days observed in the depot measurements by Watne et al. (2018), a difference potentially due to variations in en-

gine technology and the fuel types used in the bus fleets. Notably, HVO was not used in the depot study, while some buses switched from RME to HVO prior to this study. The Δ PM peaked and then decreased at higher OH_{exp}, likely due to the transition from functionalization-dominated reactions and condensation at lower OH_{exp} to fragmentation reactions and evaporation dominance at higher OH_{exp} (Tkacik et al., 2014; Ortega et al., 2016). The Δ PM in this study was comparable to 855 mg (kg fuel)⁻¹ for a mixed fleet consisting of 44.1 % gasoline, 41.3 % diesel, and 14.6 % liquefied petroleum gas (LPG) vehicles measured at an urban roadside

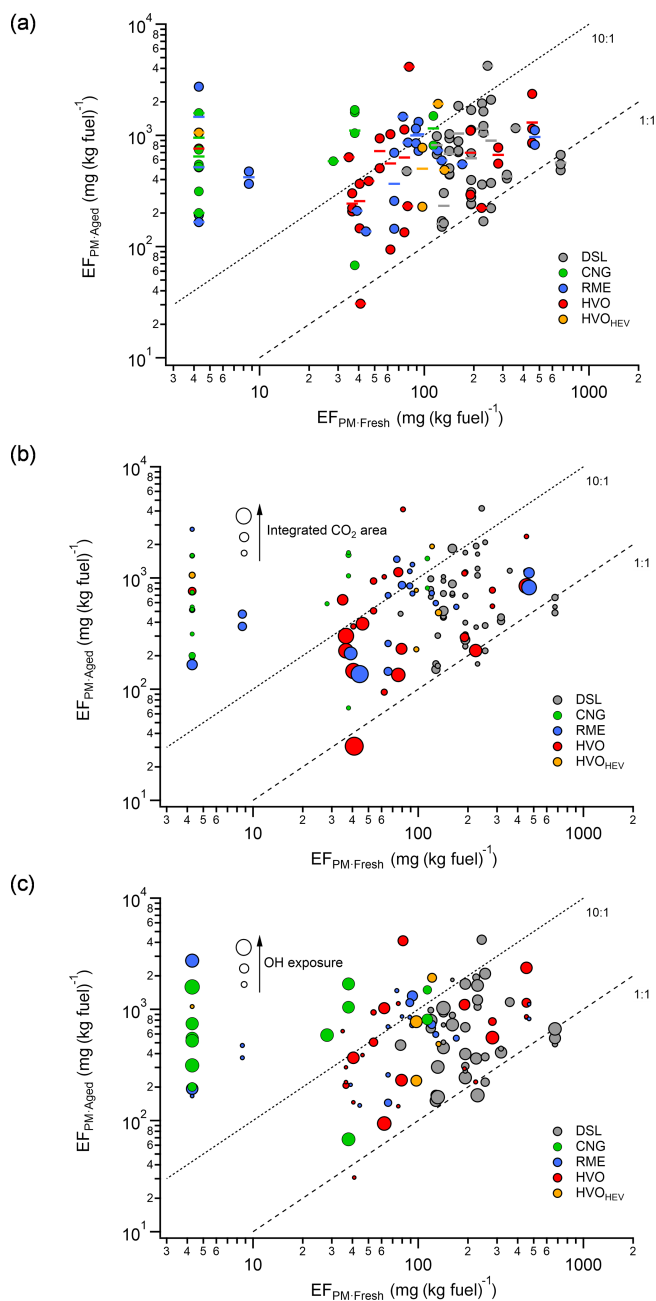


Figure 2. $EF_{PM:aged}$ vs. average $EF_{PM:fresh}$ for all the studied bus passages (Euro V) with respect to fuel type (a) and as a function of the dilution level of the plumes (integrated CO_2 area; range from 120 to 2×10^4 ppm s) (b) and OH exposure (OH_{exp} ; range from 1.1×10^9 to 4.6×10^{11} molecules cm^{-3} s) (c). The dashed lines denote the 10 : 1 and 1 : 1 $EF_{PM:aged} : EF_{PM:fresh}$ ratios, and the solid lines in panel (a) represent the bus averages. One may note that the buses with $EF_{PM:fresh}$ values below the detection limit were set to $4.3 \text{ mg}(\text{kg fuel})^{-1}$. Abbreviations: DSL (diesel), CNG (compressed natural gas), RME (rapeseed methyl ester), HVO (hydrotreated vegetable oil), and HVO_{HEV} (hybrid-electric HVO).

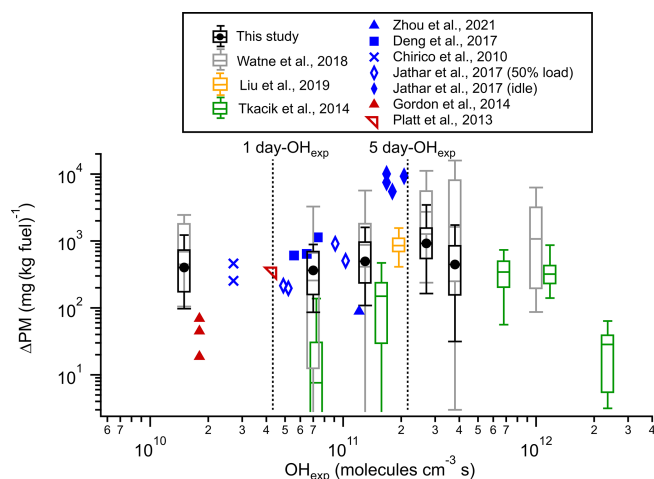


Figure 3. Secondary particle mass formed (ΔPM), calculated as the average $EF_{PM:fresh}$ subtracted from $EF_{PM:aged}$ vs. modeled OH exposure (OH_{exp}) for the bus fleet in this study and comparison with those reported for a tunnel study (Tkacik et al., 2014), a depot study (Watne et al., 2018), roadside measurements (T. Liu et al., 2019; Zhou et al., 2021), middle-duty and heavy-duty diesel vehicles (Deng et al., 2017), diesel passenger cars (Chirico et al., 2010), a diesel engine (Jathar et al., 2017a), and gasoline vehicles (Gordon et al., 2014a; Platt et al., 2013). Dashed lines indicate 1 and 5 d OH_{exp} assuming an OH concentration of 1×10^6 molecules cm^{-3} 12 h d^{-1} (Watne et al., 2018).

in Hong Kong (T. Liu et al., 2019). It was slightly higher than the ΔPM measured from a Euro-VI-dominated (more than 70 %) heavy-duty truck fleet at an urban roadside in Gothenburg (Zhou et al., 2021) and from a fleet with over 80 % light-duty gasoline vehicles in a Pittsburgh tunnel study (Tkacik et al., 2014). Additionally, the ΔPM in this study was consistent with those for middle-duty and heavy-duty diesel vehicles (Deng et al., 2017), diesel passenger cars (Chirico et al., 2010), and a diesel (or biodiesel)-fuelled engine under a 50 % load condition (Jathar et al., 2017a) (around $190\text{--}1133 \text{ mg}(\text{kg fuel})^{-1}$). However, the diesel (or biodiesel)-fuelled engine under idle conditions can produce significantly higher ΔPM (more than $5000 \text{ mg}(\text{kg fuel})^{-1}$), likely because engines at idle loads are less efficient at burning fuel, leading to higher emissions of unburned gaseous combustion products (as precursors of secondary PM) (Nordin et al., 2013; Saliba et al., 2017; Jathar et al., 2017a). In contrast, experiments conducted for gasoline vehicles at relatively low photochemical ages (< 1 OH day) typically produced a ΔPM of lower than $70 \text{ mg}(\text{kg fuel})^{-1}$ (Gordon et al., 2014a), except for a Euro V gasoline vehicle ($340 \text{ mg}(\text{kg fuel})^{-1}$) operated with the New European Driving Cycle (Platt et al., 2013).

3.2 Chemical characterization using CIMS

3.2.1 Fresh gaseous emissions

Figure 4 presents the median emission factors (M^dEFs) of acetate-CIMS-measured fresh gaseous emissions with respect to fuel type. The identities of the organic compounds detected by HR-ToF-CIMS are assigned based on knowledge of sensitivities of the ionization scheme and the expected compounds emitted from the buses. Plausible compounds are assigned from the formulae, with the caveat that other isomers might contribute to the signal. These compounds were classified into nine families based on their molecular characteristics as outlined by Liu et al. (2017), with additional details provided in the Supplement. Among all Euro V/EEV buses, hybrid-electric HVO (HVO_{HEV}) buses exhibited the highest M^dEF of CIMS-measured fresh gaseous emissions ($68 \text{ mg (kg fuel)}^{-1}$), followed by DSL ($42 \text{ mg (kg fuel)}^{-1}$), RME ($18 \text{ mg (kg fuel)}^{-1}$), and CNG ($16 \text{ mg (kg fuel)}^{-1}$), while HVO had the lowest M^dEF of $12 \text{ mg (kg fuel)}^{-1}$. Nitrogen (N)-containing compounds (no sulfur) and monoacid families predominantly composed these fresh gaseous emissions. Compared to Euro V HVO_{HEV} buses, HVO_{HEV} buses equipped with exhaust gas recirculation (EGR) and DPF systems (Euro VI) demonstrated a significant reduction in M^dEF ($10 \text{ mg (kg fuel)}^{-1}$), primarily due to decreased emissions of N-containing compounds, although the M^dEF of other compound families was higher. In contrast, Zhou et al. (2021) reported significant reductions in both carboxylic acids and carbonyl compounds (by 94 % on average) and acidic nitrogen-containing organic and inorganic species (79 %) when transitioning from Euro V to Euro VI heavy-duty trucks. However, details on the types of exhaust after-treatment systems used in the trucks from that study are not specified. Moreover, this study utilized acetate as a different reagent ion for CIMS compared to the iodide used by Zhou et al. (2021).

Table 2 lists the top 10 M^dEFs of fresh gaseous compounds, contributing over 88 % of the total fresh gaseous emissions measured by CIMS for most of the bus types, except for Euro VI HVO_{HEV} (61 %). The fresh gaseous emissions from all types of Euro V/EEV buses were primarily composed of HONO and HNO_3 , with HONO being the most significant acidic emission. The M^dEFs of HONO and HNO_3 generally align with values reported in the literature, ranging from approximately $7\text{--}250 \text{ mg (kg fuel)}^{-1}$ for HONO (Kurtenbach et al., 2001; Wentzell et al., 2013; Liao et al., 2020; Nakashima and Kondo, 2022) to approximately $4\text{--}14 \text{ mg (kg fuel)}^{-1}$ for HNO_3 (Wentzell et al., 2013). Acetic acid ($C_2H_4O_2$), formic acid (CH_2O_2), and HNCO also exhibited relatively high M^dEFs . The M^dEFs of formic acid for all Euro V/EEV bus types ($0.02\text{--}1.97 \text{ mg (kg fuel)}^{-1}$) were consistent with those from a light-duty gasoline fleet ($0.57\text{--}0.94 \text{ mg (kg fuel)}^{-1}$) reported by Crisp et al. (2014). The M^dEFs of acetic acid ranged from

1.23 to $4.84 \text{ mg (kg fuel)}^{-1}$, falling between values for gasoline vehicles ($0.78 \text{ mg (kg fuel)}^{-1}$) and diesel buses (approximately $12\text{--}23 \text{ mg (kg fuel)}^{-1}$) (Li et al., 2021). Isocyanic acid (HNCO), likely an intermediate product of the thermal degradation of urea in SCR systems without sufficient hydrolysis (Bernhard et al., 2012), was detected in emissions from all the bus types, with M^dEFs of $0.08\text{--}14.74 \text{ mg (kg fuel)}^{-1}$. These values are slightly lower than those from a non-road diesel engine ($31\text{--}56 \text{ mg (kg fuel)}^{-1}$) reported by Jathar et al. (2017b) but align well with SCR-equipped diesel vehicles tested by Suarez-Bertoa and Astorga (2016) ($1.3\text{--}9.7 \text{ mg (kg fuel)}^{-1}$) and a diesel engine with a diesel oxidation catalyst (DOC) (Wentzell et al., 2013) ($0.21\text{--}3.96 \text{ mg (kg fuel)}^{-1}$). Of all Euro V/EEV buses, HVO_{HEV} buses showed the highest emissions of HNCO, potentially attributed to cold-engine conditions since the combustion engine does not operate continuously. Notably, emissions of HNCO were significantly lowered, and neither HONO nor HNO_3 was identified among the top 10 M^dEFs for HVO_{HEV} buses equipped with EGR and DPF systems (Euro VI), suggesting that newer engine technologies incorporating EGR and DPF systems are likely effective in reducing emissions of NO_x (Table 1) as well as HNCO, HONO, and HNO_3 . CH_4SO_3 , potentially identified as methanesulfonic acid, was detected in the emissions from DSL and RME buses. Previous studies, such as those by Corrêa and Arbilla (2008), showed that mercaptans, emitted from diesel and biodiesel exhausts, can transform under high NO_x conditions into products including methanesulfonic acid. The presence of sulfur-containing organic compounds in diesel fuel and lubricants, their potential transformation upon combustion into various sulfuric derivatives, and the catalytic activity of engine converters could also contribute to such findings. However, the detailed formation pathway of CH_4SO_3 in our study remains unknown.

3.2.2 Aged gaseous emissions

Secondary carboxylic acids were measured following exposure of the exhaust to OH radicals. Figure 5 shows the correlations between ion counts of the most abundant gas-phase organic acids and HNO_3 after oxidation in Go:PAM. HNO_3 serves as an indicator of NO_x oxidation. Most acids exhibited both primary and secondary sources, except for dihydroxyacetic acid ($C_2H_4O_4$), which was only identified post aging. The chemical characterization of the aged emissions was conducted on separate occasions using HR-ToF-CIMS, capturing a limited number of buses ($N = 19$). When these buses were categorized by fuel type, the sample size for each category became smaller, constraining statistical comparison across different bus types. Nevertheless, we analyzed the relationship between various chemical species across all the buses. Glycolic acid ($C_2H_4O_3$), $C_2H_4O_4$, pyruvic acid ($C_3H_4O_3$), malonic acid ($C_3H_4O_4$), lactic acid ($C_3H_6O_3$), and acetoacetic acid ($C_4H_6O_3$) showed high correlations

Table 2. Summary of the top 10 $MdEFs$ of fresh gaseous compounds measured using HR-ToF-CIMS of DSL, CNG, RME, HVO, and HVO_{HEV} buses^a (color-coded by the different families shown in Fig. 4).

| DSL, Euro V, SCR | | CNG, EEV/Euro V | | RME, Euro V, SCR | | HVO, Euro V, SCR | | HVO _{HEV} , Euro V, SCR | | HVO _{HEV} , Euro VI | |
|--|------------------------------------|--|------------------------------------|---|------------------------------------|--|------------------------------------|---|------------------------------------|--|------------------------------------|
| Species | $MdEF$ ($mg\ kg_{fuel}^{-1}$) | Species | $MdEF$ ($mg\ kg_{fuel}^{-1}$) | Species | $MdEF$ ($mg\ kg_{fuel}^{-1}$) | Species | $MdEF$ ($mg\ kg_{fuel}^{-1}$) | Species | $MdEF$ ($mg\ kg_{fuel}^{-1}$) | Species | $MdEF$ ($mg\ kg_{fuel}^{-1}$) |
| HONO | 20.64 | HONO | 4.92 | HONO | 12.72 | HONO | 7.62 | HONO | 38.96 | C ₃ H ₂ O ₂ | 2.42 |
| HNO ₃ | 5.29 | C ₂ H ₄ O ₂ | 4.68 | HNO ₃ | 3.24 | HNO ₃ | 2.20 | HNO ₃ | 14.74 | C ₂ H ₄ O ₂ | 1.23 |
| C ₂ H ₄ O ₂ | 4.84 | HNO ₃ | 3.48 | C ₂ H ₄ O ₂ | 1.23 | C ₂ H ₄ O ₂ | 1.23 | HNO ₃ | 7.89 | C ₂ H ₂ O ₃ | 0.62 |
| CH ₂ O ₂ | 1.97 | HNO ₃ | 0.51 | CH ₂ O ₂ | 0.48 | C ₃ H ₆ O ₃ | 0.14 | C ₂ H ₄ O ₂ | 1.83 | C ₈ H ₆ O ₄ | 0.40 |
| C ₃ H ₆ O ₃ | 1.79 | CH ₂ O ₂ | 0.30 | HNO ₃ | 0.15 | C ₃ H ₂ O ₂ | 0.09 | CH ₂ O ₂ | 0.45 | C ₆ H ₅ NO ₂ | 0.31 |
| CH ₄ SO ₃ | 0.71 | C ₂ H ₂ O ₃ | 0.25 | C ₂ H ₂ O ₃ | 0.05 | HNO ₃ | 0.08 | C ₃ H ₆ O ₃ | 0.43 | HNO ₃ | 0.27 |
| HNO ₃ | 0.67 | C ₃ H ₂ O ₂ | 0.14 | C ₃ H ₈ O ₃ | 0.03 | CH ₂ O ₂ | 0.02 | C ₃ H ₂ O ₂ | 0.34 | C ₃ H ₄ O ₃ | 0.22 |
| C ₃ H ₄ O ₃ | 0.37 | C ₃ H ₄ O ₂ | 0.06 | CH ₄ SO ₃ | 0.02 | C ₂ H ₂ O ₃ | 0.02 | C ₉ H ₁₀ O ₃ | 0.16 | C ₇ H ₆ O ₃ | 0.20 |
| C ₂ H ₂ O ₃ | 0.31 | C ₇ H ₆ O ₃ | 0.05 | C ₃ H ₄ O ₂ | 0.02 | C ₃ H ₄ O ₃ | 0.02 | C ₈ H ₆ O ₄ | 0.12 | C ₃ H ₈ O ₃ | 0.17 |
| C ₄ H ₆ O ₄ | 0.22 | C ₅ H ₈ O ₄ | 0.05 | C ₆ H ₆ N ₂ O ₂ | 0.01 | C ₄ H ₆ O ₄ | 0.01 | C ₅ H ₈ O ₃ | 0.10 | H ₄ N ₂ O ₂ S | 0.16 |

^a DSL, CNG, RME, HVO, and HVO_{HEV} are the abbreviations for diesel, compressed natural gas, rapeseed methyl ester, hydrotreated vegetable oil, and hybrid-electric hydrotreated vegetable oil.

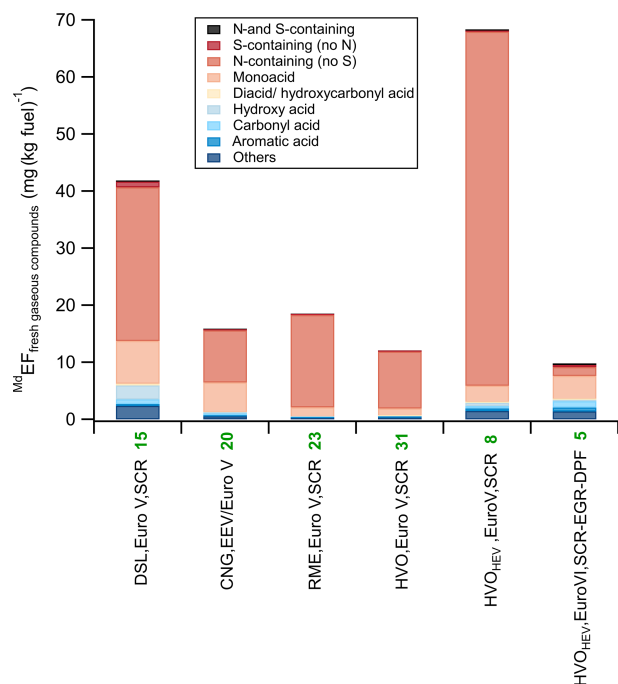


Figure 4. $MdEFs$ of CIMS-measured fresh gaseous emissions with respect to fuel class: DSL (diesel, 15), CNG (compressed natural gas, 20), RME (rapeseed methyl ester, 23), HVO (rapeseed methyl ester, 31), and HVO_{HEV} (hybrid-electric HVO, 13) buses. The number in bold green represents the number of buses examined.

($R^2 = 0.85$ – 0.99 , Fig. 5a–f) with HNO₃ signals. In contrast, glutaric acid (C₅H₈O₄) and succinic acid (C₄H₆O₄) exhibited poorer correlations with HNO₃, suggesting different formation mechanisms for these two organic acids compared to the others mentioned. Notably, these two acids showed a strong correlation with each other ($R^2 = 0.97$, Fig. 5i), and

both belong to the diacid or hydroxycarbonyl acid families. It is important to note that many of these carboxylic acids can directly participate in secondary PM formation in the atmosphere in the presence of water vapor and a base such as ammonia (Chen et al., 2020; Huang et al., 2018; Hao et al., 2020). This process may significantly contribute to the overall secondary PM yield, reflecting a more complex interplay between gaseous emissions and particulate matter under atmospheric conditions. While most of these small organic acids correlated well with HNO₃, their correlations with EF_{PM:aged} and ΔPM were moderate to weak ($R^2 < 0.6$, Fig. S5). This possibly indicates that the OH-driven formation of these carboxylic acids occurs on a different timescale compared to the production of organic aerosol (Friedman et al., 2017), at least in this Go:PAM experiment. This could also be due to different subsets of hydrocarbon precursors driving the production of organic acids and secondary particle mass. Similarly, Friedman et al. (2017) observed a lack of correlation between organic aerosol and gaseous organic acid concentrations downstream of the flow reactor from a diesel engine, indicating that organic acids may not be reliable tracers of secondary organic aerosol formation from diesel exhaust.

3.2.3 Particulate emissions

Table 3 displays the top 10 EFs of fresh particle-phase compounds (EF_{fresh}) as characterized by the FIGAERO ToF-CIMS, alongside their respective aged EFs (EF_{aged}) for the Euro V DSL and RME buses. These top 10 EF_{fresh} values contributed over 82 % of the total fresh particulate emissions measured by CIMS. Fresh particulate emissions from DSL buses were predominantly composed of H₂SO₄ and HNO₃. Benzene or toluene oxidation products (C₇H₄O₇, C₇H₈O, C₆H₅NO₃, C₆H₅O, and C₇H₇NO₃) also had a rel-

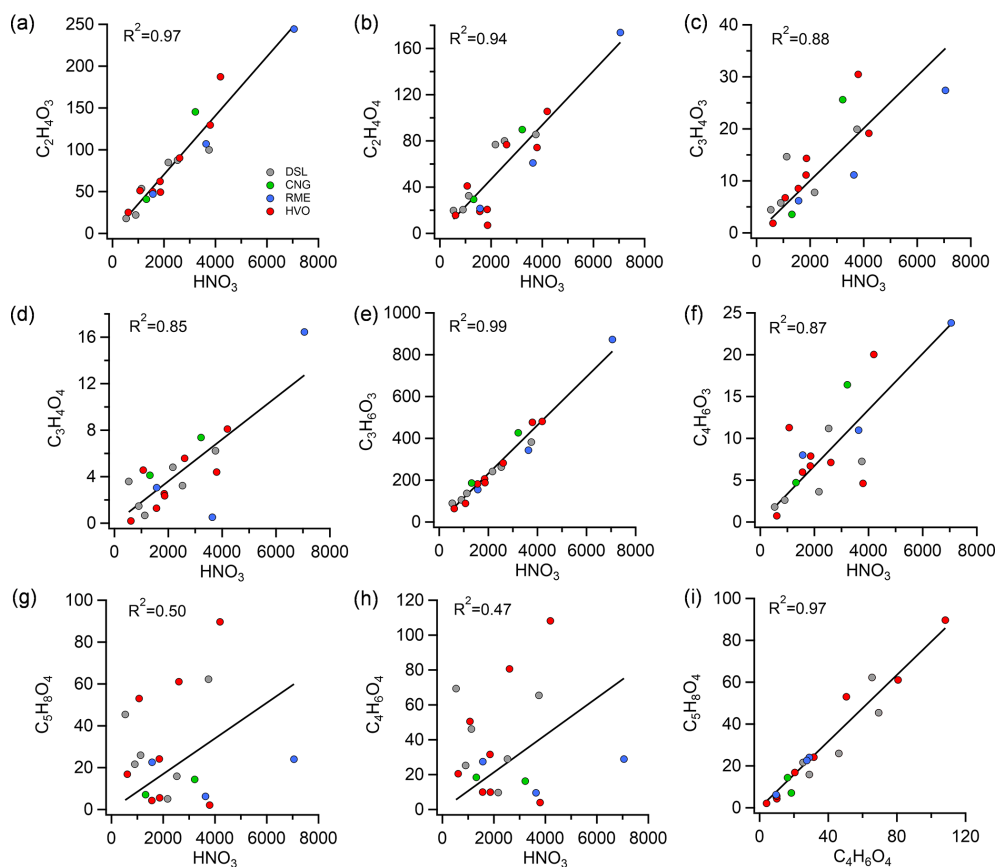


Figure 5. Correlations between ion counts of the most abundant gas-phase organic acids and HNO_3 (a–h) and the correlation between glutaric acid ($\text{C}_5\text{H}_8\text{O}_4$) and succinic acid ($\text{C}_4\text{H}_6\text{O}_4$) (i) from 19 buses after oxidation in Go:PAM. Abbreviations: DSL (diesel), CNG (compressed natural gas), RME (rapeseed methyl ester), HVO (hydrotreated vegetable oil), and HVO_{HEV} (hybrid-electric HVO).

atively high EF_{fresh} , aligning with the findings in Le Breton et al. (2019). Similarly, high EF_{fresh} values of HNO_3 ($2.5 \text{ mg (kg fuel)}^{-1}$) and H_2SO_4 ($0.61 \text{ mg (kg fuel)}^{-1}$) were observed for the RME bus. Additionally, fatty acids, known as the main components of unburned rapeseed oil (Usmanov et al., 2015), such as $\text{C}_{18}\text{H}_{34}\text{O}_2$, $\text{C}_{14}\text{H}_{28}\text{O}_2$, $\text{C}_{18}\text{H}_{36}\text{O}_2$, $\text{C}_{16}\text{H}_{32}\text{O}_2$, and $\text{C}_{16}\text{H}_{30}\text{O}_2$, significantly contributed to the identified mass loadings from the RME bus. When comparing the percentage mass observed by CIMS for both DSL and RME fuels in fresh and aged exhaust plumes, the total emission factors measured by CIMS (EF_{CIMS}) were notably lower than the total emission factors measured by the EEPS (EF_{total}). This difference is expected due to the sensitivity of the acetate ionization scheme of CIMS, which efficiently detects oxygenated volatile organic compounds, particularly carboxylic acids and inorganic acids, but it has low sensitivity to hydrocarbons and cannot detect metallic ions and soot. The CIMS-measured EF_{fresh} accounted for 10.4 % and 5.9 % of the fresh EF_{total} measured by the EEPS for DSL and RME, respectively. In aged exhaust, EF_{CIMS} represented higher percentages of EF_{total} (25.8 % for DSL and 17.9 % for

RME), likely because of an increased proportion of organics with acid groups.

4 Conclusions and atmospheric implications

To address the challenges posed by increasing transportation needs, associated greenhouse gas emissions, and related climate change impacts, biofuels have been promoted as a low-carbon alternative to fossil fuels. In 2020, for the 27 Member States of the European Union, 93.2 % of the total fuel supply for road transport was derived from fossil fuels, while 6.8 % came from biofuels, with Sweden having the highest biofuel share at 23.2 % (Vourliotakis and Platsakis, 2022). This study investigated renewable fuels like RME, HVO, and methane (when using biogas) in terms of primary emissions of pollutants and their secondary formation after photochemical aging. DSL buses without a DPF displayed the highest $\text{EF}_{\text{PM:Fresh}}$, whereas CNG buses emitted the lowest $\text{EF}_{\text{PM:Fresh}}$, with a median $\text{EF}_{\text{PM:Fresh}}$ below the detection limit. Despite there being a more than 1 order of magnitude difference in $\text{EF}_{\text{PM:Fresh}}$ between buses operated with various fuel types, we observed smaller variations in $\text{EF}_{\text{PM:aged}}$.

Table 3. Summary of the top 10 EF_{fresh} values of PM-contributing species with their respective EF_{aged} in Euro V DSL and RME emissions.

| DSL | | | RME | | |
|---|---|--|--|---|--|
| Species | EF_{fresh} (mg (kg fuel)^{-1}) | EF_{aged} (mg (kg fuel)^{-1}) | Species | EF_{fresh} (mg (kg fuel)^{-1}) | EF_{aged} (mg (kg fuel)^{-1}) |
| H ₂ SO ₄ | 4.8 | 6.8 | HNO ₃ | 2.5 | 45 |
| HNO ₃ | 3.2 | 50 | C ₁₈ H ₃₄ O ₂ | 1.2 | 0.81 |
| C ₇ H ₄ O ₇ | 1.8 | 3.8 | H ₂ SO ₄ | 0.61 | 0.68 |
| HNCO | 1.1 | 1.2 | C ₁₄ H ₂₈ O ₂ | 0.52 | 0.85 |
| C ₇ H ₈ O | 0.9 | 7.2 | HNCO | 0.45 | 0.089 |
| C ₃ H ₆ O ₃ | 0.6 | 23 | C ₁₈ H ₃₆ O ₂ | 0.32 | 0.046 |
| C ₆ H ₅ NO ₃ | 0.53 | 2.6 | C ₁₆ H ₃₂ O ₂ | 0.30 | 0.18 |
| C ₄ H ₆ O ₅ | 0.45 | 0.30 | C ₆ H ₅ O ₂ | 0.12 | 8.6 |
| C ₆ H ₅ O | 0.26 | 15.6 | C ₄ H ₆ O ₄ | 0.089 | 6.3 |
| C ₇ H ₇ NO ₃ | 0.15 | 4.6 | C ₁₆ H ₃₀ O ₂ | 0.081 | 0.012 |
| EF_{total} measured by the EEPS | 160.9 | 1289.8 | EF_{total} measured by the EEPS | 127.7 | 1320.6 |
| EF_{CIMS} | 16.8 | 320.1 | EF_{CIMS} | 7.5 | 237.2 |
| $EF_{\text{CIMS}}/EF_{\text{total}}$ (%) | 10.4 | 25.8 | $EF_{\text{CIMS}}/EF_{\text{total}}$ (%) | 5.9 | 17.9 |

suggesting that secondary particle formation is likely influenced by substantial non-fuel-dependent precursor sources such as lubrication oils and/or fuel additives. Recognizing these sources is crucial for refining regulations on hydrocarbon emissions, which could notably enhance secondary PM control. The median ratios of aged to fresh particle mass emission factors, listed in ascending order, were for diesel (4.0), HVO (6.7), HVO_{HEV} (10.5), RME (10.8), and CNG buses (84), highlighting the significant yet often overlooked contributions of aged or photochemically processed emissions to urban air quality. Furthermore, Zhao et al. (2017) revealed a strongly nonlinear relationship between SOA formation from vehicle exhaust and the ratio of non-methane organic gas to NO_x (NMOG : NO_x). For instance, increasing the NMOG : NO_x ratio from 4 to 10 ppbC/ppbNO_x increased the SOA yield from dilute gasoline vehicle exhaust by a factor of 8, underscoring the importance of integrated emission control policies for NO_x and organic gases for better managing SOA formation. While implementing regulations for secondary particle formation presents significant challenges, it is crucial for a thorough understanding of their impact on regional air quality and health. Our approach to measuring the maximum secondary PM formation potential – peaking at a photochemical age of approximately 5 equivalent days of atmospheric OH exposure – provides a possible semi-quantitative reference for comparing secondary PM formation potential across different studies. We acknowledge the limitations of this approach for direct regulatory application and emphasize the need for more precise and comprehensive research to develop a methodologically robust framework that stakeholders can agree upon for systematically assessing the impacts of vehicles on air quality and informing regulatory strategies.

It is important to note that the ambient temperature during this study was relatively low, which does not affect the EF

comparison across different buses, but one should be aware of this when comparing these results to studies conducted at significantly higher temperatures. Wang et al. (2017) noted lower particle number EFs in summer compared to winter, potentially due to increased nucleation or condensation at cooler temperatures. Temperature impacts on emissions are significant during cold starts when combustion is inefficient (Nam et al., 2010). Post warmup, soot-mode particles show little temperature sensitivity (Ristimäki et al., 2005). Book et al. (2015) found inconsistent trends in particle emissions from DPF-equipped diesel trucks across various temperatures and driving cycles, suggesting that more research is needed to understand the temperature effects on emissions from different bus types under varied operational conditions.

Non-regulated chemical species can also have serious negative impacts on air quality and human health. Organic and inorganic acids influence the pH of precipitation and will potentially contribute to acid deposition, affecting ecosystem health. Furthermore, there is a risk that some abatement systems might generate unintended compounds, such as HNCO from the thermal degradation of urea in SCR systems without sufficient hydrolysis. Additionally, Jathar et al. (2017b) observed substantial direct emissions of HNCO from diesel engines and estimated that ambient concentrations in Los Angeles could vary widely, ranging from 20 to 107 ppt depending on different parameterizations of diesel engine emissions. The persistence of HNCO in the atmosphere, particularly under dry conditions, poses significant health risks. It has been linked to severe outcomes, including respiratory and cardiovascular disorders, atherosclerosis, cataracts, and rheumatoid arthritis (Leslie et al., 2019; Roberts et al., 2011). In our study, small monoacids (C₁–C₃) and nitrogen-containing compounds, such as HONO, HNO₃, and HNCO, dominated the fresh gaseous emissions measured by acetate CIMS for all Euro V/EEV buses regardless of fuel type,

with HVO_{HEV} buses exhibiting the highest emissions. Notably, the emission levels of nitrogen-containing compounds were significantly lower in Euro VI buses, equipped with advanced after-treatment systems that include EGR and DPF technologies in addition to SCR-only techniques. This indicates that transitioning to vehicles equipped with more advanced emission control technologies can be beneficial, even though these technologies may not be specifically designed to target emissions of HONO, HNO₃, and HNCO. Consequently, a detailed evaluation of the environmental and health effects of emerging engine and after-treatment technologies is highly desirable for future considerations. Overall, the extended online chemical characterization of in-use fleet emissions, utilizing advanced techniques like HR-ToF-CIMS, enables the identification of unregulated pollutants, which is crucial for more informed policy decisions and vehicle technology developments.

Data availability. The data used in this publication are available to the community and can be accessed by request to the corresponding author.

Supplement. The supplement related to this article is available online at: <https://doi.org/10.5194/acp-24-11045-2024-supplement>.

Author contributions. ÅMH, MLB, and QL made the measurements. ÅMH designed the project, coordinated the measurements, and together with MH and CKC supervised the study. LZ, QL, MLB, CMS, and ÅMH carried out the data analysis. LZ, QL, JZY, MH, ÅMH, and CKC prepared the manuscript. All the co-authors contributed to the discussion and interpretation of the results.

Competing interests. The contact author has declared that none of the authors has any competing interests.

Disclaimer. Publisher's note: Copernicus Publications remains neutral with regard to jurisdictional claims made in the text, published maps, institutional affiliations, or any other geographical representation in this paper. While Copernicus Publications makes every effort to include appropriate place names, the final responsibility lies with the authors.

Special issue statement. This article is part of the special issue "Air quality research at street level – Part II (ACP/GMD inter-journal SI)". It is not associated with a conference.

Acknowledgements. This work was financed by VINNOVA, Sweden's Innovation Agency (grant no. 2013-03058) and Formas (grant no. 2020-01907) and was an initiative within the framework program "Photochemical smog in China" financed by the Swedish

Research Council (grant no. 639-2013-6917). Chak K. Chan would like to acknowledge the support of the National Natural Science Foundation of China (grant nos. 41675117 and 41875142).

Financial support. This work was financed by VINNOVA, Sweden's Innovation Agency (grant no. 2013-03058) and Formas (grant no. 2020-01907) and was an initiative within the framework program "Photochemical smog in China" financed by the Swedish Research Council (grant no. 639-2013-6917). Additionally, it received support from the National Natural Science Foundation of China (grant nos. 41675117 and 41875142).

Review statement. This paper was edited by Lea Hildebrandt Ruiz and reviewed by two anonymous referees.

References

- Aljawhary, D., Lee, A. K. Y., and Abbatt, J. P. D.: High-resolution chemical ionization mass spectrometry (ToF-CIMS): application to study SOA composition and processing, *Atmos. Meas. Tech.*, 6, 3211–3224, <https://doi.org/10.5194/amt-6-3211-2013>, 2013.
- Arnold, F., Pirjola, L., Ronkko, T., Reichl, U., Schlager, H., Lahde, T., Heikkilä, J., and Keskinen, J.: First online measurements of sulfuric acid gas in modern heavy-duty diesel engine exhaust: implications for nanoparticle formation, *Environ. Sci. Technol.*, 46, 11227–11234, 2012.
- Bernhard, A. M., Peitz, D., Elsener, M., Wokaun, A., and Kröcher, O.: Hydrolysis and thermolysis of urea and its decomposition byproducts biuret, cyanuric acid and melamine over anatase TiO₂, *Appl. Catal. B-Environ.*, 115, 129–137, 2012.
- Book, E. K., Snow, R., Long, T., Fang, T., and Baldauf, R.: Temperature effects on particulate emissions from DPF-equipped diesel trucks operating on conventional and biodiesel fuels, *J. Air Waste Manage.*, 65, 751–758, 2015.
- Brady, J. M., Crisp, T. A., Collier, S., Kuwayama, T., Forestieri, S. D., Perraud, V., Zhang, Q., Kleeman, M. J., Cappa, C. D., and Bertram, T. H.: Real-time emission factor measurements of isocyanic acid from light duty gasoline vehicles, *Environ. Sci. Technol.*, 48, 11405–11412, <https://doi.org/10.1021/es504354p>, 2014.
- Bruns, E. A., El Haddad, I., Keller, A., Klein, F., Kumar, N. K., Pieber, S. M., Corbin, J. C., Slowik, J. G., Brune, W. H., Baltensperger, U., and Prévôt, A. S. H.: Inter-comparison of laboratory smog chamber and flow reactor systems on organic aerosol yield and composition, *Atmos. Meas. Tech.*, 8, 2315–2332, <https://doi.org/10.5194/amt-8-2315-2015>, 2015.
- Chen, L., Bao, Z., Wu, X., Li, K., Han, L., Zhao, X., Zhang, X., Wang, Z., Azzi, M., and Cen, K.: The effects of humidity and ammonia on the chemical composition of secondary aerosols from toluene / NO_x photo-oxidation, *Sci. Total Environ.*, 728, 138671, <https://doi.org/10.1016/j.scitotenv.2020.138671>, 2020.
- Chirico, R., DeCarlo, P. F., Heringa, M. F., Tritscher, T., Richter, R., Prévôt, A. S. H., Dommen, J., Weingartner, E., Wehrle, G., Gysel, M., Laborde, M., and Baltensperger, U.: Impact of aftertreatment devices on primary emissions and secondary organic aerosol formation potential from in-use diesel vehi-

- cles: results from smog chamber experiments, *Atmos. Chem. Phys.*, 10, 11545–11563, <https://doi.org/10.5194/acp-10-11545-2010>, 2010.
- Corrêa, S. M. and Arbilla, G.: Mercaptans emissions in diesel and biodiesel exhaust, *Atmos. Environ.*, 42, 6721–6725, 2008.
- Crisp, T. A., Brady, J. M., Cappa, C. D., Collier, S., Forestieri, S. D., Kleeman, M. J., Kuwayama, T., Lerner, B. M., Williams, E. J., and Zhang, Q.: On the primary emission of formic acid from light duty gasoline vehicles and ocean-going vessels, *Atmos. Environ.*, 98, 426–433, 2014.
- Deng, W., Hu, Q., Liu, T., Wang, X., Zhang, Y., Song, W., Sun, Y., Bi, X., Yu, J., Yang, W., Huang, X., Zhang, Z., Huang, Z., He, Q., Mellouki, A., and George, C.: Primary particulate emissions and secondary organic aerosol (SOA) formation from idling diesel vehicle exhaust in China, *Sci. Total Environ.*, 593–594, 462–469, <https://doi.org/10.1016/j.scitotenv.2017.03.088>, 2017.
- Edwards, R., Mahieu, V., Griesemann, J.-C., Larivé, J.-F., and Rickard, D. J.: Well-to-wheels analysis of future automotive fuels and powertrains in the European context, *SAE Transactions*, 113, 1072–1084, <https://www.jstor.org/stable/44740827> (last access: 18 December 2023), 2004.
- Emanuelsson, E. U., Hallquist, M., Kristensen, K., Glasius, M., Bohn, B., Fuchs, H., Kammer, B., Kiendler-Scharr, A., Nehr, S., Rubach, F., Tillmann, R., Wahner, A., Wu, H.-C., and Mentel, Th. F.: Formation of anthropogenic secondary organic aerosol (SOA) and its influence on biogenic SOA properties, *Atmos. Chem. Phys.*, 13, 2837–2855, <https://doi.org/10.5194/acp-13-2837-2013>, 2013.
- Energimyndigheten: Energy in Sweden 2021 – An Overview, <https://www.energimyndigheten.se/en/news/2021/an-overview-of-energy-in-sweden-2021-now-available/> (last access: December 2023), 2021.
- Fitzmaurice, H. L. and Cohen, R. C.: A method for using stationary networks to observe long-term trends of on-road emission factors of primary aerosol from heavy-duty vehicles, *Atmos. Chem. Phys.*, 22, 15403–15411, <https://doi.org/10.5194/acp-22-15403-2022>, 2022.
- Friedman, B., Link, M. F., Fulgham, S. R., Brophy, P., Galang, A., Brune, W. H., Jathar, S. H., and Farmer, D. K.: Primary and Secondary Sources of Gas-Phase Organic Acids from Diesel Exhaust, *Environ. Sci. Technol.*, 51, 10872–10880, <https://doi.org/10.1021/acs.est.7b01169>, 2017.
- Fullerton, D. G., Bruce, N., and Gordon, S. B.: Indoor air pollution from biomass fuel smoke is a major health concern in the developing world, *T. Roy. Soc. Trop. Med. H.*, 102, 843–851, 2008.
- Gentner, D. R., Jathar, S. H., Gordon, T. D., Bahreini, R., Day, D. A., El Haddad, I., Hayes, P. L., Pieber, S. M., Platt, S. M., and de Gouw, J.: Review of urban secondary organic aerosol formation from gasoline and diesel motor vehicle emissions, *Environ. Sci. Technol.*, 51, 1074–1093, 2017.
- Giechaskiel, B., Riccobono, F., Vlachos, T., Mendoza-Villafuerte, P., Suarez-Bertoa, R., Fontaras, G., Bonnel, P., and Weiss, M.: Vehicle emission factors of solid nanoparticles in the laboratory and on the road using portable emission measurement systems (PEMS), *Frontiers in Environmental Science*, 3, 82, <https://doi.org/10.3389/fenvs.2015.00082>, 2015.
- Gordon, T. D., Presto, A. A., May, A. A., Nguyen, N. T., Lipsky, E. M., Donahue, N. M., Gutierrez, A., Zhang, M., Maddox, C., Rieger, P., Chattopadhyay, S., Maldonado, H., Maricq, M. M., and Robinson, A. L.: Secondary organic aerosol formation exceeds primary particulate matter emissions for light-duty gasoline vehicles, *Atmos. Chem. Phys.*, 14, 4661–4678, <https://doi.org/10.5194/acp-14-4661-2014>, 2014a.
- Gordon, T. D., Presto, A. A., Nguyen, N. T., Robertson, W. H., Na, K., Sahay, K. N., Zhang, M., Maddox, C., Rieger, P., Chattopadhyay, S., Maldonado, H., Maricq, M. M., and Robinson, A. L.: Secondary organic aerosol production from diesel vehicle exhaust: impact of aftertreatment, fuel chemistry and driving cycle, *Atmos. Chem. Phys.*, 14, 4643–4659, <https://doi.org/10.5194/acp-14-4643-2014>, 2014b.
- Guerreiro, C. B., Foltescu, V., and De Leeuw, F.: Air quality status and trends in Europe, *Atmos. Environ.*, 98, 376–384, 2014.
- Hak, C. S., Hallquist, M., Ljungstrom, E., Svane, M., and Pettersson, J. B. C.: A new approach to in-situ determination of roadside particle emission factors of individual vehicles under conventional driving conditions, *Atmos. Environ.*, 43, 2481–2488, <https://doi.org/10.1016/j.atmosenv.2009.01.041>, 2009.
- Hallquist, Å. M., Jerksjö, M., Fallgren, H., Westerlund, J., and Sjödin, Å.: Particle and gaseous emissions from individual diesel and CNG buses, *Atmos. Chem. Phys.*, 13, 5337–5350, <https://doi.org/10.5194/acp-13-5337-2013>, 2013.
- Hallquist, M., Wenger, J. C., Baltensperger, U., Rudich, Y., Simpson, D., Claeys, M., Dommen, J., Donahue, N. M., George, C., Goldstein, A. H., Hamilton, J. F., Herrmann, H., Hoffmann, T., Iinuma, Y., Jang, M., Jenkin, M. E., Jimenez, J. L., Kiendler-Scharr, A., Maenhaut, W., McFiggans, G., Mentel, Th. F., Monod, A., Prévôt, A. S. H., Seinfeld, J. H., Surratt, J. D., Szmigielski, R., and Wildt, J.: The formation, properties and impact of secondary organic aerosol: current and emerging issues, *Atmos. Chem. Phys.*, 9, 5155–5236, <https://doi.org/10.5194/acp-9-5155-2009>, 2009.
- Hao, L., Kari, E., Leskinen, A., Worsnop, D. R., and Virtanen, A.: Direct contribution of ammonia to α -pinene secondary organic aerosol formation, *Atmos. Chem. Phys.*, 20, 14393–14405, <https://doi.org/10.5194/acp-20-14393-2020>, 2020.
- Hassaneen, A., Munack, A., Ruschel, Y., Schroeder, O., and Krahl, J.: Fuel economy and emission characteristics of Gas-to-Liquid (GTL) and Rapeseed Methyl Ester (RME) as alternative fuels for diesel engines, *Fuel*, 97, 125–130, 2012.
- Huang, M., Xu, J., Cai, S., Liu, X., Hu, C., Gu, X., Zhao, W., Fang, L., and Zhang, W.: Chemical analysis of particulate products of aged 1, 3, 5-trimethylbenzene secondary organic aerosol in the presence of ammonia, *Atmos. Pollut. Res.*, 9, 146–155, 2018.
- Janhäll, S. and Hallquist, M.: A novel method for determination of size-resolved, submicrometer particle traffic emission factors, *Environ. Sci. Technol.*, 39, 7609–7615, <https://doi.org/10.1021/es048208y>, 2005.
- Jathar, S. H., Friedman, B., Galang, A. A., Link, M. F., Brophy, P., Volckens, J., Eluri, S., and Farmer, D. K.: Linking load, fuel, and emission controls to photochemical production of secondary organic aerosol from a diesel engine, *Environ. Sci. Technol.*, 51, 1377–1386, 2017a.
- Jathar, S. H., Heppding, C., Link, M. F., Farmer, D. K., Akherati, A., Kleeman, M. J., de Gouw, J. A., Veres, P. R., and Roberts, J. M.: Investigating diesel engines as an atmospheric source of isocyanic acid in urban areas, *Atmos. Chem. Phys.*, 17, 8959–8970, <https://doi.org/10.5194/acp-17-8959-2017>, 2017b.

- Ježek, I., Drinovec, L., Ferrero, L., Carriero, M., and Močnik, G.: Determination of car on-road black carbon and particle number emission factors and comparison between mobile and stationary measurements, *Atmos. Meas. Tech.*, 8, 43–55, <https://doi.org/10.5194/amt-8-43-2015>, 2015.
- Kang, E., Root, M. J., Toohey, D. W., and Brune, W. H.: Introducing the concept of Potential Aerosol Mass (PAM), *Atmos. Chem. Phys.*, 7, 5727–5744, <https://doi.org/10.5194/acp-7-5727-2007>, 2007.
- Kawamura, K., Ng, L. L., and Kaplan, I. R.: Determination of organic acids (C1–C10) in the atmosphere, motor exhausts, and engine oils, *Environ. Sci. Technol.*, 19, 1082–1086, 1985.
- Kawamura, K. and Kaplan, I. R.: Motor exhaust emissions as a primary source for dicarboxylic acids in Los Angeles ambient air, *Environ. Sci. Technol.*, 21, 105–110, 1987.
- Kirchstetter, T. W., Harley, R. A., and Littlejohn, D.: Measurement of nitrous acid in motor vehicle exhaust, *Environ. Sci. Technol.*, 30, 2843–2849, 1996.
- Kroll, J. H., Smith, J. D., Che, D. L., Kessler, S. H., Worsnop, D. R., and Wilson, K. R.: Measurement of fragmentation and functionalization pathways in the heterogeneous oxidation of oxidized organic aerosol, *Phys. Chem. Chem. Phys.*, 11, 8005–8014, 2009.
- Kuittinen, N., McCaffery, C., Peng, W., Zimmerman, S., Roth, P., Simonen, P., Karjalainen, P., Keskinen, J., Cocker, D. R., and Durbin, T. D.: Effects of driving conditions on secondary aerosol formation from a GDI vehicle using an oxidation flow reactor, *Environ. Pollut.*, 282, 117069, <https://doi.org/10.1016/j.envpol.2021.117069>, 2021.
- Kurtenbach, R., Becker, K., Gomes, J., Kleffmann, J., Lörzer, J., Spittler, M., Wiesen, P., Ackermann, R., Geyer, A., and Platt, U.: Investigations of emissions and heterogeneous formation of HONO in a road traffic tunnel, *Atmos. Environ.*, 35, 3385–3394, 2001.
- Kwak, J. H., Kim, H. S., Lee, J. H., and Lee, S. H.: On-Road Chasing Measurement of Exhaust Particle Emissions from Diesel, Cng Lpg and Dme-Fueled Vehicles Using a Mobile Emission Laboratory, *Int. J. Auto. Tech. Kor.*, 15, 543–551, <https://doi.org/10.1007/s12239-014-0057-z>, 2014.
- Lambe, A. T., Ahern, A. T., Williams, L. R., Slowik, J. G., Wong, J. P. S., Abbatt, J. P. D., Brune, W. H., Ng, N. L., Wright, J. P., Croasdale, D. R., Worsnop, D. R., Davidovits, P., and Onasch, T. B.: Characterization of aerosol photooxidation flow reactors: heterogeneous oxidation, secondary organic aerosol formation and cloud condensation nuclei activity measurements, *Atmos. Meas. Tech.*, 4, 445–461, <https://doi.org/10.5194/amt-4-445-2011>, 2011.
- Le Breton, M., Wang, Y., Hallquist, Å. M., Pathak, R. K., Zheng, J., Yang, Y., Shang, D., Glasius, M., Bannan, T. J., Liu, Q., Chan, C. K., Percival, C. J., Zhu, W., Lou, S., Topping, D., Wang, Y., Yu, J., Lu, K., Guo, S., Hu, M., and Hallquist, M.: Online gas- and particle-phase measurements of organosulfates, organosulfonates and nitrooxy organosulfates in Beijing utilizing a FIGAERO ToF-CIMS, *Atmos. Chem. Phys.*, 18, 10355–10371, <https://doi.org/10.5194/acp-18-10355-2018>, 2018.
- Le Breton, M., Psichoudaki, M., Hallquist, M., Watne, Å., Lutz, A., and Hallquist, Å.: Application of a FIGAERO ToF CIMS for online characterization of real-world fresh and aged particle emissions from buses, *Aerosol Sci. Tech.*, 53, 244–259, 2019.
- Leslie, M. D., Ridoli, M., Murphy, J. G., and Borduas-Dedekind, N.: Isocyanic acid (HNCO) and its fate in the atmosphere: a review, *Environ. Sci. Proc. Imp.*, 21, 793–808, 2019.
- Li, T., Wang, Z., Yuan, B., Ye, C., Lin, Y., Wang, S., Yuan, Z., Zheng, J., and Shao, M.: Emissions of carboxylic acids, hydrogen cyanide (HCN) and isocyanic acid (HNCO) from vehicle exhaust, *Atmos. Environ.*, 247, 118218, <https://doi.org/10.1016/j.atmosenv.2021.118218>, 2021.
- Liao, K., Chen, Q., Liu, Y., Li, Y. J., Lambe, A. T., Zhu, T., Huang, R.-J., Zheng, Y., Cheng, X., and Miao, R.: Secondary Organic Aerosol Formation of Fleet Vehicle Emissions in China: Potential Seasonality of Spatial Distributions, *Environ. Sci. Technol.*, 55, 7276–7286, <https://doi.org/10.1021/acs.est.0c08591>, 2021.
- Liao, S., Zhang, J., Yu, F., Zhu, M., Liu, J., Ou, J., Dong, H., Sha, Q., Zhong, Z., and Xie, Y.: High gaseous nitrous acid (HONO) emissions from light-duty diesel vehicles, *Environ. Sci. Technol.*, 55, 200–208, 2020.
- Link, M. F., Friedman, B., Fulgham, R., Brophy, P., Galang, A., Jathar, S. H., Veres, P., Roberts, J. M., and Farmer, D. K.: Photochemical processing of diesel fuel emissions as a large secondary source of isocyanic acid (HNCO), *Geophys. Res. Lett.*, 43, 4033–4041, <https://doi.org/10.1002/2016gl068207>, 2016.
- Liu, Q., Hallquist, Å. M., Fallgren, H., Jerksjö, M., Jutterström, S., Salberg, H., Hallquist, M., Le Breton, M., Pei, X., and Pathak, R. K.: Roadside assessment of a modern city bus fleet: Gaseous and particle emissions, *Atmos. Environ.*, X, 3, 100044, <https://doi.org/10.1016/j.aeaoa.2019.100044>, 2019.
- Liu, S., Thompson, S. L., Stark, H., Ziemann, P. J., and Jimenez, J. L.: Gas-phase carboxylic acids in a university classroom: Abundance, variability, and sources, *Environ. Sci. Technol.*, 51, 5454–5463, 2017.
- Liu, T., Wang, X., Deng, W., Hu, Q., Ding, X., Zhang, Y., He, Q., Zhang, Z., Lü, S., Bi, X., Chen, J., and Yu, J.: Secondary organic aerosol formation from photochemical aging of light-duty gasoline vehicle exhausts in a smog chamber, *Atmos. Chem. Phys.*, 15, 9049–9062, <https://doi.org/10.5194/acp-15-9049-2015>, 2015.
- Liu, T., Zhou, L., Liu, Q., Lee, B. P., Yao, D., Lu, H., Lyu, X., Guo, H., and Chan, C. K.: Secondary Organic Aerosol Formation from Urban Roadside Air in Hong Kong, *Environ. Sci. Technol.*, 53, 3001–3009, <https://doi.org/10.1021/acs.est.8b06587>, 2019.
- Lopez-Hilfiker, F. D., Mohr, C., Ehn, M., Rubach, F., Kleist, E., Wildt, J., Mentel, Th. F., Carrasquillo, A. J., Daumit, K. E., Hunter, J. F., Kroll, J. H., Worsnop, D. R., and Thornton, J. A.: Phase partitioning and volatility of secondary organic aerosol components formed from α -pinene ozonolysis and OH oxidation: the importance of accretion products and other low volatility compounds, *Atmos. Chem. Phys.*, 15, 7765–7776, <https://doi.org/10.5194/acp-15-7765-2015>, 2015.
- Lopez-Hilfiker, F. D., Mohr, C., Ehn, M., Rubach, F., Kleist, E., Wildt, J., Mentel, Th. F., Lutz, A., Hallquist, M., Worsnop, D., and Thornton, J. A.: A novel method for online analysis of gas and particle composition: description and evaluation of a Filter Inlet for Gases and AEROSols (FIGAERO), *Atmos. Meas. Tech.*, 7, 983–1001, <https://doi.org/10.5194/amt-7-983-2014>, 2014.
- Martinet, S., Liu, Y., Louis, C., Tassel, P., Perret, P., Chaumond, A., and Andre, M.: Euro 6 unregulated pollutant characterization and statistical analysis of after-treatment device and driving-

- condition impact on recent passenger-car emissions, *Environ. Sci. Technol.*, 51, 5847–5855, 2017.
- May, A. A., Nguyen, N. T., Presto, A. A., Gordon, T. D., Lipsky, E. M., Karve, M., Gutierrez, A., Robertson, W. H., Zhang, M., Brandow, C., Chang, O., Chen, S. Y., Cicero-Fernandez, P., Dinkins, L., Fuentes, M., Huang, S. M., Ling, R., Long, J., Maddox, C., Massetti, J., McCauley, E., Miguel, A., Na, K., Ong, R., Pang, Y. B., Rieger, P., Sax, T., Truong, T., Vo, T., Chatopadhyay, S., Maldonado, H., Maricq, M. M., and Robinson, A. L.: Gas- and particle-phase primary emissions from in-use, on-road gasoline and diesel vehicles, *Atmos. Environ.*, 88, 247–260, <https://doi.org/10.1016/j.atmosenv.2014.01.046>, 2014.
- Millet, D. B., Baasandorj, M., Farmer, D. K., Thornton, J. A., Baumann, K., Brophy, P., Chaliyakunnel, S., de Gouw, J. A., Graus, M., Hu, L., Koss, A., Lee, B. H., Lopez-Hilfiker, F. D., Neuman, J. A., Paulot, F., Peischl, J., Pollack, I. B., Ryerson, T. B., Warneke, C., Williams, B. J., and Xu, J.: A large and ubiquitous source of atmospheric formic acid, *Atmos. Chem. Phys.*, 15, 6283–6304, <https://doi.org/10.5194/acp-15-6283-2015>, 2015.
- Mohr, C., Lopez-Hilfiker, F. D., Yli-Juuti, T., Heitto, A., Lutz, A., Hallquist, M., D'Ambro, E. L., Rissanen, M. P., Hao, L., and Schobesberger, S.: Ambient observations of dimers from terpene oxidation in the gas phase: Implications for new particle formation and growth, *Geophys. Res. Lett.*, 44, 2958–2966, 2017.
- Nakashima, Y. and Kondo, Y.: Nitrous acid (HONO) emission factors for diesel vehicles determined using a chassis dynamometer, *Sci. Total Environ.*, 806, 150927, <https://doi.org/10.1016/j.scitotenv.2021.150927>, 2022.
- Nam, E., Kishan, S., Baldauf, R. W., Fulper, C. R., Sabisch, M., and Warila, J.: Temperature effects on particulate matter emissions from light-duty, gasoline-powered motor vehicles, *Environ. Sci. Technol.*, 44, 4672–4677, 2010.
- Nordin, E. Z., Eriksson, A. C., Roldin, P., Nilsson, P. T., Carlsson, J. E., Kajos, M. K., Hellén, H., Wittbom, C., Rissler, J., Löndahl, J., Swietlicki, E., Svenningsson, B., Bohgard, M., Kulmala, M., Hallquist, M., and Pagels, J. H.: Secondary organic aerosol formation from idling gasoline passenger vehicle emissions investigated in a smog chamber, *Atmos. Chem. Phys.*, 13, 6101–6116, <https://doi.org/10.5194/acp-13-6101-2013>, 2013.
- Ortega, A. M., Hayes, P. L., Peng, Z., Palm, B. B., Hu, W., Day, D. A., Li, R., Cubison, M. J., Brune, W. H., Graus, M., Warneke, C., Gilman, J. B., Kuster, W. C., de Gouw, J., Gutiérrez-Montes, C., and Jimenez, J. L.: Real-time measurements of secondary organic aerosol formation and aging from ambient air in an oxidation flow reactor in the Los Angeles area, *Atmos. Chem. Phys.*, 16, 7411–7433, <https://doi.org/10.5194/acp-16-7411-2016>, 2016.
- Palm, B. B., Campuzano-Jost, P., Ortega, A. M., Day, D. A., Kaser, L., Jud, W., Karl, T., Hansel, A., Hunter, J. F., Cross, E. S., Kroll, J. H., Peng, Z., Brune, W. H., and Jimenez, J. L.: In situ secondary organic aerosol formation from ambient pine forest air using an oxidation flow reactor, *Atmos. Chem. Phys.*, 16, 2943–2970, <https://doi.org/10.5194/acp-16-2943-2016>, 2016.
- Paulot, F., Wunch, D., Crouse, J. D., Toon, G. C., Millet, D. B., DeCarlo, P. F., Vigouroux, C., Deutscher, N. M., González Abad, G., Notholt, J., Warneke, T., Hannigan, J. W., Warneke, C., de Gouw, J. A., Dunlea, E. J., De Mazière, M., Griffith, D. W. T., Bernath, P., Jimenez, J. L., and Wennberg, P. O.: Importance of secondary sources in the atmospheric budgets of formic and acetic acids, *Atmos. Chem. Phys.*, 11, 1989–2013, <https://doi.org/10.5194/acp-11-1989-2011>, 2011.
- Pflaum, H., Hofmann, P., Geringer, B., and Weissel, W.: Potential of hydrogenated vegetable oil (HVO) in a modern diesel engine, SAE Technical Paper, 2010-32-0081, <https://doi.org/10.4271/2010-32-0081>, 2010.
- Pirjola, L., Karl, M., Rönkkö, T., and Arnold, F.: Model studies of volatile diesel exhaust particle formation: are organic vapours involved in nucleation and growth?, *Atmos. Chem. Phys.*, 15, 10435–10452, <https://doi.org/10.5194/acp-15-10435-2015>, 2015.
- Pirjola, L., Dittrich, A., Niemi, J. V., Saarikoski, S., Timonen, H., Kuuluvainen, H., Jarvinen, A., Kousa, A., Ronkko, T., and Hillamo, R.: Physical and Chemical Characterization of Real-World Particle Number and Mass Emissions from City Buses in Finland, *Environ. Sci. Technol.*, 50, 294–304, <https://doi.org/10.1021/acs.est.5b04105>, 2016.
- Platt, S. M., El Haddad, I., Zardini, A. A., Clairotte, M., Astorga, C., Wolf, R., Slowik, J. G., Temime-Roussel, B., Marchand, N., Ježek, I., Drinovec, L., Močnik, G., Möhler, O., Richter, R., Barmet, P., Bianchi, F., Baltensperger, U., and Prévôt, A. S. H.: Secondary organic aerosol formation from gasoline vehicle emissions in a new mobile environmental reaction chamber, *Atmos. Chem. Phys.*, 13, 9141–9158, <https://doi.org/10.5194/acp-13-9141-2013>, 2013.
- Preble, C. V., Dallmann, T. R., Kreisberg, N. M., Hering, S. V., Harley, R. A., and Kirchstetter, T. W.: Effects of Particle Filters and Selective Catalytic Reduction on Heavy-Duty Diesel Drayage Truck Emissions at the Port of Oakland, *Environ. Sci. Technol.*, 49, 8864–8871, <https://doi.org/10.1021/acs.est.5b01117>, 2015.
- Ristimäki, J., Keskinen, J., Virtanen, A., Maricq, M., and Aakko, P.: Cold temperature PM emissions measurement: Method evaluation and application to light duty vehicles, *Environ. Sci. Technol.*, 39, 9424–9430, 2005.
- Roberts, J. M., Veres, P. R., Cochran, A. K., Warneke, C., Burling, I. R., Yokelson, R. J., Lerner, B., Gilman, J. B., Kuster, W. C., and Fall, R.: Isocyanic acid in the atmosphere and its possible link to smoke-related health effects, *P. Natl. Acad. Sci. USA*, 108, 8966–8971, 2011.
- Saliba, G., Saleh, R., Zhao, Y., Presto, A. A., Lambe, A. T., Frodin, B., Sardar, S., Maldonado, H., Maddox, C., and May, A. A.: Comparison of gasoline direct-injection (GDI) and port fuel injection (PFI) vehicle emissions: emission certification standards, cold-start, secondary organic aerosol formation potential, and potential climate impacts, *Environ. Sci. Technol.*, 51, 6542–6552, 2017.
- Simonen, P., Saukko, E., Karjalainen, P., Timonen, H., Bloss, M., Aakko-Saksa, P., Rönkkö, T., Keskinen, J., and Dal Maso, M.: A new oxidation flow reactor for measuring secondary aerosol formation of rapidly changing emission sources, *Atmos. Meas. Tech.*, 10, 1519–1537, <https://doi.org/10.5194/amt-10-1519-2017>, 2017.
- Suarez-Bertoa, R. and Astorga, C.: Isocyanic acid and ammonia in vehicle emissions, *Transport. Res. D-Tr. E.*, 49, 259–270, 2016.
- Tkacik, D. S., Lambe, A. T., Jathar, S., Li, X., Presto, A. A., Zhao, Y. L., Blake, D., Meinardi, S., Jayne, J. T., Croteau, P. L., and Robinson, A. L.: Secondary Organic Aerosol Formation from in-Use Motor Vehicle Emissions Using a Potential

- Aerosol Mass Reactor, *Environ. Sci. Technol.*, 48, 11235–11242, <https://doi.org/10.1021/es502239v>, 2014.
- Tong, Z., Li, Y., Lin, Q., Wang, H., Zhang, S., Wu, Y., and Zhang, K. M.: Uncertainty investigation of plume-chasing method for measuring on-road NO_x emission factors of heavy-duty diesel vehicles, *J. Hazard. Mater.*, 424, 127372, <https://doi.org/10.1016/j.jhazmat.2021.127372>, 2022.
- Usmanov, R. A., Mazanov, S. V., Gabitova, A. R., Miftakhova, L. K., Gumerov, F. M., Musin, R. Z., and Abdulgatov, I. M.: The effect of fatty acid ethyl esters concentration on the kinematic viscosity of biodiesel fuel, *J. Chem. Eng. Data*, 60, 3404–3413, 2015.
- Vogt, R., Scheer, V., Casati, R., and Benter, T.: On-road measurement of particle emission in the exhaust plume of a diesel passenger car, *Environ. Sci. Technol.*, 37, 4070–4076, 2003.
- Vourliotakis, G. and Platsakis, O.: ETC CM report 2022/02: Greenhouse gas intensities of transport fuels in the EU in 2020 – Monitoring under the Fuel Quality Directive, European Topic Centre on Climate change mitigation, <https://www.eionet.europa.eu/etcs/etc-cm/products/etc-cm-report-2022-02> (last access: December 2023), 2022.
- Wang, H., Wu, Y., Zhang, K. M., Zhang, S., Baldauf, R. W., Snow, R., Deshmukh, P., Zheng, X., He, L., and Hao, J.: Evaluating mobile monitoring of on-road emission factors by comparing concurrent PEMS measurements, *Sci. Total Environ.*, 736, 139507, <https://doi.org/10.1016/j.scitotenv.2020.139507>, 2020.
- Wang, J. M., Jeong, C.-H., Zimmerman, N., Healy, R. M., Hilker, N., and Evans, G. J.: Real-world emission of particles from vehicles: volatility and the effects of ambient temperature, *Environ. Sci. Technol.*, 51, 4081–4090, 2017.
- Wang, Z., Nicholls, S. J., Rodriguez, E. R., Kummu, O., Hörkkö, S., Barnard, J., Reynolds, W. F., Topol, E. J., DiDonato, J. A., and Hazen, S. L.: Protein carbamylation links inflammation, smoking, uremia and atherogenesis, *Nat. Med.*, 13, 1176–1184, 2007.
- Watne, A. K., Psychoudaki, M., Ljungstrom, E., Le Breton, M., Hallquist, M., Jerksjo, M., Fallgren, H., Jutterstrom, S., and Hallquist, A. M.: Fresh and Oxidized Emissions from In-Use Transit Buses Running on Diesel, Biodiesel, and CNG, *Environ. Sci. Technol.*, 52, 7720–7728, <https://doi.org/10.1021/acs.est.8b01394>, 2018.
- Wentzell, J. J., Liggio, J., Li, S. M., Vlasenko, A., Staebler, R., Lu, G., Poitras, M. J., Chan, T., and Brook, J. R.: Measurements of gas phase acids in diesel exhaust: a relevant source of HNCO?, *Environ. Sci. Technol.*, 47, 7663–7671, <https://doi.org/10.1021/es401127j>, 2013.
- Yao, D., Guo, H., Lyu, X., Lu, H., and Huo, Y.: Secondary organic aerosol formation at an urban background site on the coastline of South China: Precursors and aging processes, *Environ. Pollut.*, 309, 119778, <https://doi.org/10.1016/j.envpol.2022.119778>, 2022.
- Yuan, B., Veres, P. R., Warneke, C., Roberts, J. M., Gilman, J. B., Koss, A., Edwards, P. M., Graus, M., Kuster, W. C., Li, S.-M., Wild, R. J., Brown, S. S., Dubé, W. P., Lerner, B. M., Williams, E. J., Johnson, J. E., Quinn, P. K., Bates, T. S., Lefer, B., Hayes, P. L., Jimenez, J. L., Weber, R. J., Zamora, R., Ervens, B., Millet, D. B., Rappenglück, B., and de Gouw, J. A.: Investigation of secondary formation of formic acid: urban environment vs. oil and gas producing region, *Atmos. Chem. Phys.*, 15, 1975–1993, <https://doi.org/10.5194/acp-15-1975-2015>, 2015.
- Zervas, E., Montagne, X., and Lahaye, J.: Emission of specific pollutants from a compression ignition engine. Influence of fuel hydro-treatment and fuel/air equivalence ratio, *Atmos. Environ.*, 35, 1301–1306, 2001a.
- Zervas, E., Montagne, X., and Lahaye, J.: C₁–C₅ organic acid emissions from an SI engine: Influence of fuel and air/fuel equivalence ratio, *Environ. Sci. Technol.*, 35, 2746–2751, <https://doi.org/10.1021/es000237v>, 2001b.
- Zhang, R., Suh, I., Zhao, J., Zhang, D., Fortner, E. C., Tie, X., Molina, L. T., and Molina, M. J.: Atmospheric new particle formation enhanced by organic acids, *Science*, 304, 1487–1490, 2004.
- Zhao, Y., Saleh, R., Saliba, G., Presto, A. A., Gordon, T. D., Drozd, G. T., Goldstein, A. H., Donahue, N. M., and Robinson, A. L.: Reducing secondary organic aerosol formation from gasoline vehicle exhaust, *P. Natl. Acad. Sci. USA*, 114, 6984–6989, 2017.
- Zhao, Y., Lambe, A. T., Saleh, R., Saliba, G., and Robinson, A. L.: Secondary Organic Aerosol Production from Gasoline Vehicle Exhaust: Effects of Engine Technology, Cold Start, and Emission Certification Standard, *Environ. Sci. Technol.*, 52, 1253–1261, <https://doi.org/10.1021/acs.est.7b05045>, 2018.
- Zhou, L., Hallquist, Å. M., Hallquist, M., Salvador, C. M., Gaita, S. M., Sjödin, Å., Jerksjö, M., Salberg, H., Wängberg, I., Melqvist, J., Liu, Q., Lee, B. P., and Chan, C. K.: A transition of atmospheric emissions of particles and gases from on-road heavy-duty trucks, *Atmos. Chem. Phys.*, 20, 1701–1722, <https://doi.org/10.5194/acp-20-1701-2020>, 2020.
- Zhou, L., Salvador, C. M., Priestley, M., Hallquist, M., Liu, Q., Chan, C. K., and Hallquist, Å. M.: Emissions and secondary formation of air pollutants from modern heavy-duty trucks in real-world traffic—chemical characteristics using on-line mass spectrometry, *Environ. Sci. Technol.*, 55, 14515–14525, 2021.